Reliability Engineering and System Safety 266 (2026) 111730



Contents lists available at ScienceDirect

Reliability Engineering and System Safety

journal homepage: www.elsevier.com/locate/ress



Analysis of RUL dynamics and uncertainty via time transformation

Pierre Dersin [a,*], Roberto Rocchetta [b]

[a] Division of Operations & Maintenance Engineering, Luleå University of Technology, Luleå, 971 87, Sweden
[b] University of Applied Sciences and Arts of Southern Switzerland (SUPSI-DACD), Via Flora Ruchat-Roncati 15, Mendrisio, 6850, Switzerland

ARTICLE INFO

Keywords:
Remaining useful life
PHM
Time transformation
Confidence interval
Mean residual life
Degradation
Uncertainty

ABSTRACT

This work introduces a novel analytical method to analyze the dynamics of remaining useful life (RUL) and quantify uncertainty in its estimation. The approach employs a time transformation that makes the mean residual life (MRL) a linear function of transformed time, enabling the derivation of explicit RUL confidence bounds. Once mapped back to physical space, the bounds quantify aleatoric (stochastic) uncertainty in RUL and yield asymmetrical confidence intervals for both parametric and non-parametric lifetime distributions. The approach leverages a key feature of reliability distributions: the average RUL loss rate, k, in transformed time, facilitating a direct derivation of confidence bounds. In parametric cases, k is uniquely defined by the reliability distribution parameters, while for non-parametric distributions, it is derived from data by estimating the coefficient of variation. Higher slopes indicate faster degradation, leading to narrower confidence intervals and lower RUL variance. The method's applicability to stochastic processes and robustness under different data volumes are also investigated and discussed. The novel approach reveals heretofore unknown insights into classical reliability distributions. It is demonstrated through real-world applications, including LED reliability assessment, parallel system RUL estimation, and turbofan lifespan prediction using NASA N-CMAPSS data, offering a new perspective on the evolving dynamics of mean residual life and remaining useful life.

1. Introduction

In recent years, prognostics and health management (PHM) frameworks have emerged as promising approaches to intelligent maintenance of critical systems, such as those developed in the aerospace, automotive, railway, energy, and manufacturing industries. The main objective of PHM is to ensure the reliable, safe, and cost-effective operation of systems by detecting and diagnosing degradation or faults at an early stage and predicting the RUL of the system. To achieve this objective, three types of approaches are typically employed: data-driven, [1,2], physics-based, [3–5], and hybrid, [6–9]. For reviews of PHM approaches, the interested reader is referred to [10,11].

When dealing with RUL, it is important to take into account two properties: (i) it is dynamic, that is, the RUL is a function of time, and (ii) it is uncertain. Sources of uncertainty are generally divided into two main groups:

- **Epistemic:** Related to lack of knowledge, imprecision, vague information, insufficient data, and modeling. This uncertainty is reducible when more data, better knowledge, and information are collected.
- **Aleatoric:** Due to natural variability, noise in the data, stochasticity, and randomness in an environment and monitored processes. This uncertainty can be quantified and characterized, but it is in principle not reducible by collecting more data.

Examples illustrating the need for uncertainty quantification include electric unmanned aerial vehicles and railway wheel maintenance [12,13]. In both cases, health management systems benefit from accurate RUL estimates to prevent failures, whether from mid-flight battery depletion or excessive wheel wear. Overestimating RUL can lead to safety-critical events such as flight termination, crashes, or derailments, while underestimation results in unnecessary maintenance and higher costs. These examples highlight the need for balancing safety, costs, and health management with a better understanding of RUL dynamics and uncertainty.

In prognostic and health management, accuracy is critical [14] and neglecting uncertainty can introduce significant risks. Overestimating RUL, with an optimistic prognosis, can lead to missed failures and safety hazards. On the other hand, underestimating it (a pessimistic prognosis) results in premature maintenance and economic losses. Without an uncertainty estimate, RUL predictions offer limited value to practitioners. Since RUL is inherently uncertain due to varying operational and environmental conditions and differences in degradation rates [14], several methods have been developed to account for

* Corresponding author.
E-mail addresses: pierre.dersin@ltu.se (P. Dersin), roberto.rocchetta@supsi.ch (R. Rocchetta).

https://doi.org/10.1016/j.ress.2025.111730
Received 28 August 2024; Received in revised form 20 August 2025; Accepted 16 September 2025
Available online 22 September 2025
0951-8320/© 2025 The Authors. Published by Elsevier Ltd. This is an open access article under the CC BY license (http://creativecommons.org/licenses/by/4.0/).

Nomenclature

t	Time variable
t'	Transformed time
T	Lifetime random variable
T'	Transformed lifetime random variable
$f_T(t)$	PDF of variable T
$F_T(t)$	CDF of variable T
$R_T(t)$	Survival or reliability function
$\lambda(t)$	Failure (hazard) rate at time t
B_α	α-quantile of T
μ_T or μ	Mean Time to Failure (MTTF)
RUL(t)	Remaining useful life at time t
$v(t)$	Mean residual life at time t
k	Slope parameter (linked to cv)
cv	Coefficient of variation
$g(t)$	Time transformation function
$t^\star$	Inflection point
$\boldsymbol{X}(t \mid \boldsymbol{S}, \theta)$	Degradation process
$\boldsymbol{S}$	Vector of stressors
$h(t \mid \boldsymbol{S}, \theta)$	Degradation model
ϵ	Residual noise
α	Confidence parameter
$[s^-, s^+]$	RUL interval in the transformed time
$[L_\alpha, U_\alpha]$	RUL interval at a level α
T_p	Time to reach degradation level p
$R_p(t)$	Survival for reaching level p
τ	Temperature

Abbreviations

MTTF	Mean (operating) Time to Failure
MRL	Mean Residual Life
MAE	Mean Absolute Error
TTF	Time to Failure
RUL	Remaining Useful Life
PHM	Prognostics and Health Management
PDF	Probability Density Function
CDF	Cumulative Distribution Function
UQ	Uncertainty Quantification
LED	Light Emitting Diode
NN	Neural Network
ML	Machine Learning
KDE	Kernel Density Estimate

this stochasticity. Approaches include statistical and machine learning techniques such as Bayesian models [15], neural networks [16–19], fuzzy [20,21], and other data-driven fault predictors [7,22,23]. Data-driven and physics-based approaches have complementary advantages and limitations. Data-driven methods rely heavily on the quality and quantity of available data and data augmentation techniques [24]. However, their efficiency can be limited on PHM of very durable and reliable systems with scarce failure data [25,26]. This limitation has motivated ongoing efforts to integrate both paradigms into physics-informed machine learning frameworks [27], such as methods that constrain learning models via physical laws [3], or train networks to solve uncertain physical equations [28], and other strategies [29].

In all cases, uncertainty quantification (UQ) is paramount for reliable RUL estimation and characterizing both natural variability in component lifetimes and epistemic uncertainty [30]. Despite increasing interest in UQ for ML approaches for PHM, as in [31–34], most methods still rely on simplifying assumptions and fail to capture both stochasticity and epistemic uncertainty while providing confidence bounds for RUL. Furthermore, systems and components age at varying rates due to dynamic degradation mechanisms and changing operational or environmental conditions. For instance, in lithium-ion batteries, degradation accelerates with both age and usage [34], while in mechanical components such as bearings, wear may increase under heavy loads and slow under lighter conditions [6]. In general, the loss of MRL either accelerates or decelerates over time. In some cases, applying a simple time transformation, such as a logarithmic scale for exponentially degrading systems, can linearize non-linear trends. This greatly simplifies RUL prediction and UQ. The key challenge lies in defining a time transformation that generalizes across degradation patterns. A well-chosen transformation can map non-linear MRL behavior into a domain where the MRL evolves linearly, enabling the use of simple extrapolation even when the underlying MRL loss process is complex. Once established, such a transformation can facilitate consistent RUL prediction and support decision-making processes such as condition-based maintenance and optimal scheduling, even when failure-time distributions are unknown or variable across units.

Technically, the way this is accomplished in this work is by mapping the time-to-failure distribution into a family of distributions characterized by a special property, which is that their MRL, the conditional expectation of the residual life, is a linear function of time. With that family of distributions, called the Hall-Wellner distributions [35], closed-form expressions are easily obtained for confidence intervals around the RUL. Mapping a TTF probability distribution into one belonging to the special family is performed through a nonlinear time transformation. Then, explicit expressions available in the special case are transformed into equivalent expressions in the original setting, using the inverse time transformation. We demonstrate the proposed method on an RUL estimation problem for LEDs [36], for estimating the reliability of a fleet of parallel systems [37], and on a data set from the New Commercial Aero Propulsion System Simulation (N-CMAPSS) [38]. As the proposed method enables quantification of uncertainty for the RUL using closed-form expressions for time-dependent confidence bounds, it provides invaluable support for predictive maintenance (supporting the definition of risk reduction actions, preventing system failures) and also data collection decision-making.

This work introduces a novel analytical framework for estimating dynamic RUL that connects lifetime loss dynamics to uncertainty in the lifetime variability. The framework enables direct derivation of confidence intervals for RUL, enhancing uncertainty quantification. By employing a time transformation technique, the MRL becomes a linear function of transformed time, making it possible to explicitly derive confidence bounds and identify the inflection time, a point when the rate of change in failure or survival is the highest. Confidence bounds are derived analytically in the linearized case and then mapped to the original time using an inverse time transformation. The time transformation leaves the first and second-order moments invariant and gives valuable insights into asset reliability and RUL uncertainty. This procedure yields RUL confidence intervals that are distribution-free, non-symmetric, and time-variant, and it is thus applicable to a wide range of PHM problems and both parametric and non-parametric reliability distributions. The slope of the mean residual life in the transformed distribution has a one-to-one correspondence with the coefficient of variation of the time-to-failure and characterizes both uncertainty and degradation speed. Also, note that an inflection time can be derived using the proposed method, and this information is particularly valuable for supporting maintenance, accelerated testing, data collection, and other prognostic-related decision-making processes. The significance of this approach for dynamic RUL estimation, real-time monitoring, and maintenance optimization is highlighted and discussed in this work as a promising avenue for future research, particularly in complex systems analysis and concurrent failure modes. The time transformation has interesting geometrical properties that bring new

insights into the degradation process, which are not apparent with classical methods. The authors believe it could be a nexus linking data-driven and physics-based approaches, a subject for future study.

The main contributions of this work can be summarized as follows:

- A novel non-parametric time-transformation that maps arbitrary time-to-failure distributions into a domain where the mean residual life is linear, while preserving first- and second-order moments.
- An analytical derivation of time-variant, asymmetric, and non-linear (possibly non-monotonic) RUL confidence bounds that obviate the need for sampling-based estimation (bootstrap or Monte-Carlo). This is a lightweight, closed-form methodology suitable for online prognostics, enabling real-time uncertainty quantification in condition-based maintenance systems.
- Degradation dynamics and aleatoric uncertainty are characterized thanks to the estimated slope of the transformed MRL, including variations in the aging process via identification of inflection points. New geometric insights into classical reliability laws (e.g., Weibull, exponential, gamma) obtained through the time-warp framework.
- Empirical validation on LED lumen-depreciation, parallel-system reliability, and N-CMAPSS turbofan data demonstrates efficacy and accuracy of the approach.

The remainder of this paper is organized as follows: Section 2 presents the mathematical background, and Section 3 presents an overview of uncertainty-related issues in PHM. Section 4 presents the novel approach adopted in this work. Three case studies are presented in Section 5, and the numerical results are presented and discussed. Section 6 presents a concise discussion of the numerical results, whilst Section 7 closes the paper with conclusions and recommendations for future research.

2. Mathematical background

2.1. Survival distribution

The time-to-failure, or lifetime, defines the moment in time when a system or component no longer satisfies given functionality requirements [1], e.g., when a key performance indicator reaches an unacceptable degradation level [39]. We define the lifetime (time to failure) as T and its cumulative distribution function (CDF) as:

$$F_T(t) = \int_0^t f_T(u)\,du = \mathbb{P}[T \le t]. \tag{1}$$

where $F_T(t)$ is the unreliability of the device at time t, i.e., the probability of facing failures/unacceptable performance before time t. The reliability of the system is simply the probability $\mathbb{P}[T > t]$ and the reliability/survival function $R_T(t)$ is defined by, $R_T(t) = 1 - F_T(t)$. The failure rate, or hazard rate, is the conditional probability of failure per unit of time after a failure-free period t :

$$\lambda(t) = \frac{f_T(t)}{R_T(t)} = -\frac{d}{dt}\log(R_T(t)) \tag{2}$$

and the survival function can be conveniently rewritten as the exponential of the negative cumulative hazard, as

$$R_T(t) = \exp\left(-\int_0^t \lambda(u)du\right) \tag{3}$$

The alpha-level quantile of T can be obtained by inverting the lifetime CDF as follows:

$$B_\alpha = F_T^{-1}(\alpha) \tag{4}$$

where $\alpha \in [0, 1]$ is the probability level defining the percentage of failed devices.

2.2. Mean time-to-failure, RUL, and MRL

The mean lifetime, or MTTF, can be obtained directly from the reliability function as follows:

$$\mu_T = \mathbb{E}[T] = \int_0^\infty R_T(t)\,dt = \int_0^\infty t f_T(t)\,dt. \tag{5}$$

On the other hand, the mean residual life MRL, or mean RUL $v(t)$, is given by the conditional expectation of residual useful life as follows:

$$v(t) = \mathbb{E}[(T-t) \mid T \ge t] = \frac{\int_t^\infty R_T(u)\,du}{R_T(t)}. \tag{6}$$

where $\mathrm{RUL}(t) = (T - t)$ is the remaining useful life. Note that $\mathrm{RUL}(t)$ is a random variable, and $v(t)$ is a time-varying quantity as it depends on the condition $T \ge t$ on the survival time, hence conditioning on the assets that survived at least until time t. In particular, the following relationship is useful:

$$\frac{dv}{dt} = \lambda(t)v(t) - 1 \tag{7}$$

where Eq. (7) characterizes changes over time in the MRL.

A perfect knowledge or estimation of any of $R(t)$, $\lambda(t)$, or $v(t)$ determines the others precisely [40]. However, perfect estimation is only achieved asymptotically, and thus epistemic uncertainty always affects these quantities, e.g., due to limited failure data, censoring, and incomplete information. Statistical and generalized probabilistic models have been proposed to address this challenge, e.g., [26], and accelerated degradation tests are often applied, [41–43], ultimately reducing the epistemic uncertainty affecting the estimated lifetime distributions.

2.3. Accelerated degradation models

In practice, assets and components might experience different failure and degradation processes resulting from simultaneous exposure to multiple stresses. Accelerated degradation analysis seeks statistical inferences on the mutual effect of multiple factors on the durability of critical components. Let us define a non-linear degradation process by:

$$\mathbf{X}(t|\mathbf{S}, \theta) = h(t|\mathbf{S}, \theta) + \epsilon \tag{8}$$

where $\mathbf{X} \in \mathbb{R}^{n_x}$ are n_x degradation indicators which depend on a vector of stressors $\mathbf{S} = (S_1, \ldots, S_{n_S}) \in \mathcal{S}$, e.g., current, temperature, vibrations, and parameters θ defining the fitting coefficients of a non-linear degradation model $h(t|\mathbf{S}, \theta)$. $\mathcal{S}$ is the space of accelerated factors. The term ϵ is a random noise term which, in principle, can be heteroscedastic in the time domain and in the space $\mathcal{S}$, e.g., when noise increases over time or when higher/lower stress levels increase/decrease the variance of $\mathbf{X}$. To ease the analysis, we will assume ϵ in Eq. (8) to be invariant across time and within the space of the stressor values.

3. Uncertainty in PHM

PHM frameworks generally need to perform RUL predictions under uncertainty and partial knowledge of the underlying processes that drive system degradation, performance loss, and failures. To address these challenges, several researchers have proposed different approaches for RUL prediction using various techniques such as Bayesian inference, [15,44], neural networks, [17,18], fuzzy logic, [21], and data-driven models. In recent years, the focus of research in PHM has shifted towards ML-based techniques [27] for handling large and complex data sets. However, the effectiveness of ML-based approaches depends largely on the quality and quantity of data available for training and testing models. Also, the PHM community is increasingly aware that, besides the prediction of a point estimate for the RUL, it is highly desirable to provide uncertainty bounds. Work in that direction has followed two paths: model-based and data-driven approaches. When a

physics-based model is available, [13] has used first-order and inverse first-order reliability methods to derive probability bounds on the RUL analytically, using a state-space model, and under specific assumptions (typically, Gaussian distribution and constant amplitude loading). More recently [45] has surveyed various deep learning methods that enable uncertainty quantification to some extent, such as Deep Gaussian Processes, Monte Carlo dropout, and ensemble methods, and have illustrated them on case studies and characterized their efficiency.

Data fusion techniques have been extensively explored to address the challenges of reducing epistemic uncertainty, with frameworks such as those in [7,46–48] demonstrating effectiveness in handling heterogeneous data sources across various applications. For example, [46] provides an overview of uncertainty quantification and reduction techniques applied to LED reliability assessment, along with a classification of accelerated stress tests. In [47], RUL uncertainty bounds are derived by integrating multi-source accelerated degradation testing datasets, effectively addressing dataset discrepancies to enhance degradation analysis and prescribe bounded reliability functions. In [48], a Gaussian-evidential hidden Markov model is proposed to blend domain knowledge with condition monitoring information. Finally, [7] presents a robust model selection framework that leverages heterogeneous data to mitigate failure data scarcity in the design of fault detection models. The approach proposed in our work, similar to [47], focuses on prescribing uncertainty bounds on the RUL. However, unlike [47], the RUL bounds proposed are derived analytically and quantify/bound the remaining useful life variability (aleatoric uncertainty) rather than epistemic uncertainty caused by inconsistent multi-source datasets. The analytical formulation presented here establishes a direct relationship between the slope of the MRL in a transformed time domain and the shape factor of well-known reliability distributions, such as Weibull and Gamma. This explicit relationship is interpretable, an essential quality for the trustworthiness of a prognostic approach [49].

Uncertainty bounds for the RUL are generally expressed as probabilistic bounds in the form

$$\mathbb{P}\big(\mathrm{RUL}(t) \in [a, b]\big) = 1 - \alpha, \tag{9}$$

where $1 - \alpha$ is the selected confidence level, see e.g. [50]. The type of bounds in Eq. (9) is precise (tight) as they hold with an equality sign. This equality ensures that the bound holds exactly at the chosen probabilistic level. When the available data is limited, however, the increased epistemic uncertainty renders such precise estimates less reliable. In those cases, uncertainty bounds are often formulated using an inequality to provide a conservative guarantee. Specifically, non-asymptotic bounds are expressed as two-level probability statements, e.g., as in [30] :

$$1 - \overline{\alpha} \leq \mathbb{P}\left(\mathrm{RUL}(t) \in [a, b]\right) \leq 1 - \underline{\alpha} \tag{10}$$

where an imprecise probability bound is assigned on the probability statement, e.g., accounting for both aleatoric uncertainty and the epistemic uncertainty arising from limited data and model complexity. For a detailed discussion on probabilistic bounds and their relationship to sample size, confidence level, and the complexity of probabilistic statements, refer to [7,51,52].

This paper introduces a new semi-analytical approach to derive RUL bounds in the first form efficiently and for any distribution. Note that the bounds are generally based on underlying assumptions on the RUL probability distribution, for instance, characterized by its conditional MRL, variance, and type of family. This distribution represents the aleatoric uncertainty and natural variability inherent in the failure process, which cannot be reduced by further data collection. The distribution parameters (and family) are estimated from data and, while they can be estimated more accurately by gathering additional observations, they are never known exactly, i.e., only in the asymptotic limit with an infinite number of samples. This source of uncertainty, known as epistemic uncertainty, implies that the bounds a and b of the confidence interval are functions of these imperfectly known parameters and the assumptions about the underlying failure distribution. This aspect should be considered throughout the analysis, even if not explicitly reiterated in this work. Future work will extend the present study by developing robust, data-dependent uncertainty bounds, as exemplified by Eq. (10).

4. The proposed methodology

Recently, a new approach based on the estimation of degradation level has been introduced by the first author for RUL prediction [14]. This approach combines classical reliability engineering techniques with an innovative time transformation that maps the TTF data to a space where MRL is a linear function of time, which allows for explicit closed-form expressions for the confidence intervals around the RUL.

This new methodology consists of three key steps:

- **Step 1:** Run-to-failure data is collected, and the properties of probability distributions with MRL linear in time are used. Those distributions are rescaled Beta distributions for which explicit confidence intervals and RUL expressions can be derived.
- **Step 2:** A time transformation process $t' = g(t)$, named time warping, universally converts any time-to-failure distribution into a space where $v(t')$ linear in t'.
- **Step 3:** By leveraging the outcomes from the initial steps, confidence bounds, denoted by $[s^-, s^+]$, are computed in the transformed time t'. The derived confidence interval is then transformed back to the original time domain through the inverse of the time warping g^{-1}, and RUL confidence intervals are derived.

Fig. 1 illustrates the key steps of the new methodology in a conceptual flowchart, alongside an illustrative example. First, run-to-failure data are obtained from degradation paths (through estimating first passage times in the top panel). Then, the parameters of a time transformation function are estimated from data and subsequently applied to ensure linear MRL (step 2). Finally, in Step 3, the RUL confidence intervals are determined in the transformed time, i.e., such that $RUL(t') \in [s^-, s^+]$ with probability $1 - \alpha$, and then transformed to the original time scale using the inverse of the time transformation function. This procedure yields confidence intervals for the RUL at a given time t, that is, a bound $\mathrm{RUL}(t) \in [L_\alpha(t), U_\alpha(t)]$ with confidence $1 - \alpha$.

In contrast with much of the existing literature, the proposed approach does not rely on assumptions about the RUL distribution family. In contrast to much of the existing literature, the resulting confidence bounds are time-dependent, non-linear (possibly non-monotonic), and asymmetric. Hence, the bounds can be expressed as non-linear functions of the survival time. Albeit they always encompass the true (unknown) mean residual life, they may not always be centered on it. While the TTF distribution can be non-parametric, we assume it to be precisely known. This assumption is crucial for applying the time transformation g, and it represents a limitation of the proposed approach, especially in scenarios where epistemic uncertainty is significant, such as with high censoring rates or severe data scarcity. Extending this framework to account for distributional and parametric imprecision due to epistemic uncertainties is a promising direction, and it is left to future research. In the next section, we present a formal analysis of the MRL distribution in the transformed time domain and the derivation of the corresponding RUL confidence bounds, which are central to the proposed methodology.

4.1. Special case where MRL is a linear function of time

Consider the special case where MRL is a linear function of time characterized by two parameters μ and k:

$$v(t) = \mu - kt, \tag{11}$$

where μ is the mean time to failure, i.e., the expectation of the RUL at time $t = 0$, and the slope k is the expected RUL loss rate per unit of

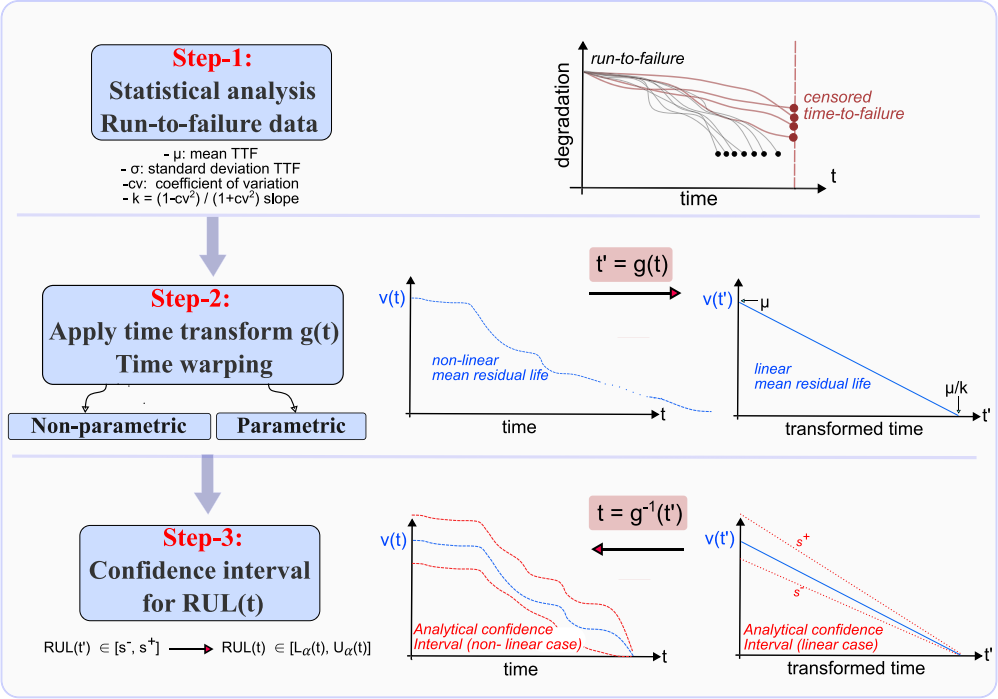


Fig. 1. A flowchart summarizing the main steps of the method adopted in this work.

time and relates to the speed of aging. In this special case, the failure rate $\lambda(t)$ is immediately derived from Eq. (7) as:

$$\lambda(t) = \frac{1-k}{\mu - kt}. \tag{12}$$

Then, from Eq. (3), the reliability function is derived:

$$R(t) = (1 - \frac{kt}{\mu})^{\frac{1-k}{k}} \tag{13}$$

This family of TTF distributions was first studied by Hall and Wellner [35,53], who demonstrated that, for $0 < k < 1$, they correspond to re-scaled Beta distributions, whereas for $k = 0$ they reduce to the exponential distribution.

From the reliability function (13), confidence intervals for the RUL are immediately derived [14]. A straightforward calculation leads to the following relationship between the slope, or degradation rate, k, and the coefficient of variation cv of the RUL:

$$k = \frac{1 - cv^2}{1 + cv^2} \tag{14}$$

where by definition, $cv = \frac{\sigma}{\mu}$, where σ is the standard deviation of the time-to-failure. The relation in Eq. (14) shows that for $cv < 1$, the smaller the coefficient of variation cv, the faster the degradation, i.e., the larger the parameter k. Hence, the uncertainty in the RUL and degradation speed are antagonistic, a behavior that confirms the intuition.

Interestingly, when MRL is linear, confidence intervals for the RUL can be derived analytically [14]. Let us describe the confidence interval for the RUL, at a $(1-\alpha)$ confidence level, the upper and lower bounds s^+ and s^- are defined as follows:

$$s^+(t) = \left(\frac{\mu}{k} - t\right) \cdot \left[1 - \left(\frac{\alpha}{2}\right)^{\frac{k}{1-k}}\right], \tag{15}$$

$$s^-(t) = \left(\frac{\mu}{k} - t\right) \cdot \left[1 - \left(1 - \frac{\alpha}{2}\right)^{\frac{k}{1-k}}\right]. \tag{16}$$

Note that the confidence bounds decrease linearly in time and the interval $[s^-, s^+]$ is symmetric only for $k = 0.5$, which corresponds to a uniform distribution. In fact, it is seen that the confidence interval is generally asymmetric, not centered around the mean residual life $v(t)$. For $k > 0.5$ the upper bound is closer to the mean than the lower bound whilst for $k < 0.5$ the opposite holds. In Eqs. (15)–(16), the parameters μ and k must be estimated from data and are therefore affected by epistemic uncertainty. A formal characterization of that uncertainty is not explicitly addressed in this work and the interested reader is referred to, e.g., [1,54–56].

Fig. 2 illustrates this behavior for a component with an initial MRL of $\mu = 100$ h at $t = 0$, evaluated for seven values of the confidence parameter α. The left panel shows the dependence of confidence interval width on the slope parameter k, while the right panel depicts the asymmetric bounds given by Eqs. (15) and (16). Note that fast aging, i.e., higher values of the slope parameter k, produces lower uncertainty in the RUL estimated and narrower confidence intervals.

4.2. Time transformation for nonlinear MRL

In general, the mean residual life is not a linear function of time. Nonetheless, it is possible, as shown in [14], to introduce a time transformation $g(t)$ to map the lifetime variable t to a warped lifetime t' so that the MRL linearly decreases in the transformed domain. Formally, the transformed MRL is expressed as,

$$v(t') = \mu - kt' = \mu - kg(t), \tag{17}$$

where $t' = g(t)$ is a time warping function and k determines the speed of aging (loss of MRL) in the transformed space.

Time warping function: The transformation is expressed in terms of the reliability function $R(t)$ by, [14],

$$g(t) = \frac{\mu}{k}\left(1 - R(t)^{\frac{k}{1-k}}\right), \tag{18}$$

where the parameter k is defined by the coefficient of variation as in Eq. (14). The expression for $g(t)$ results from imposing the constraint that the reliability function remains invariant under the time warping, i.e., $R'(g(t)) = R(t)$. Then, one can apply the known Eqs. (15)–(16) for the special case of MRL linear in time t'. By using the inverse time transformation $t = g^{-1}(t')$, confidence bounds in the initial time t can be derived. The interested reader is referred to Appendix B for proof that the $g(t)$ transformation leaves the first- and second-order moments invariant, and to [14] for additional details and examples.

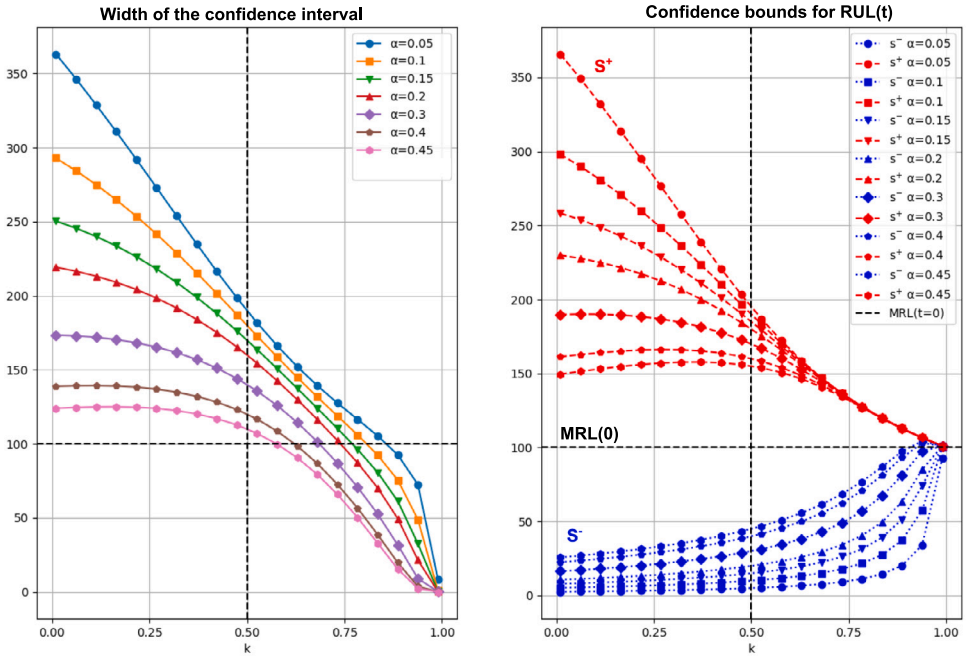


Fig. 2. Left panel: Reduction in the width $s^+ - s^-$ of the RUL interval with increasing k and various confidence levels α. **Right panel:** Upper and lower bounds as functions of k and α. Both panels present results for $t = 0$ and $v(0) = 100$ h, as specified in the Eqs. (15), (16).

4.2.1. Physical interpretation of the time transformation

The transformation $g(t)$ makes the MRL a linear function of the transformed time whilst the instantaneous rate, dg/dt, is a dilation factor, that is, when $dg/dt > 1$, each time step in the real world contributes more to "aging", and when $dg/dt < 1$, each time step counts for less. Physically, dg/dt represents the rate of change in degradation speed over operating time. For instance, if over a time range a crack's growth rate accelerates (as in many fatigue processes), dg/dt must increase to keep the crack advance uniform in the transformed time domain (and therefore MRL linear in that transformed time). The g function is then convex over that time range since dg/dt is increasing. Conversely, if damage progresses more slowly because crack growth enters a stable-propagation regime, then dg/dt decreases to account for this, and $g(t)$ is concave over the corresponding time range. Thus, the trend of dg/dt directly reflects whether the system's wearout is accelerating or slowing down. In the limiting case of constant wear-out, $dg/dt = 1$ (for $t < \frac{\mu}{k}$) and MRL is linear in time (with slope $-k$). Points in time when the wear-out trend shifts from speeding up to slowing down correspond to inflection points of the g function (where it shifts from convex to concave or vice versa). Finally, note that g reaches an asymptote when t goes to infinity, $R(t)$ converges to 0, and $g(t)$ converges to a positive constant ($\frac{\mu}{k}$), so that $\lim_{t\to\infty} dg/dt = 0$. In other words, asymptotically, an additional time step contributes no marginal increase in wear-out.

4.3. Derivation of a confidence interval for the RUL

A confidence interval for the RUL will now be constructed by using the nonlinear time transformation just introduced. Consider some t and $\mathrm{RUL}(t) = T' - t$. It is desired to build a confidence interval around $\mathrm{RUL}(t)$ for general cases, starting from the transformed time t'. The bounds in Eqs. (15) and (16), can be transformed to the original time. This yields Theorem 1 stated below.

Theorem 1. *Let the lifetime distribution be characterized by the time transformation $g(\cdot)$, as defined in Eqs. (18) and (14). Then, the $(1-\alpha)$-level confidence interval for the remaining useful life at time t is:*

$$RUL(t) \in [L_\alpha(t), U_\alpha(t)] \tag{19}$$

where

$$L_\alpha(t) = g^{-1}\left[\frac{\mu}{k}\left(1 - f_L(\alpha,k)\right) + g(t) f_L(\alpha,k)\right] - t, \tag{20}$$

$$U_\alpha(t) = g^{-1}\left[\frac{\mu}{k}\left(1 - f_U(\alpha,k)\right) + g(t) f_U(\alpha,k)\right] - t, \tag{21}$$

with $f_L(\alpha,k) = \left(1 - \frac{\alpha}{2}\right)^{\frac{k}{1-k}}$ *and* $f_U(\alpha,k) = \left(\frac{\alpha}{2}\right)^{\frac{k}{1-k}}$.

We start the proof by realizing that the transformed time t' has a mean residual life that is a linear function by construction and, consequently, the confidence interval $[s^-(t'), s^+(t')]$ can be calculated analytically. For confidence level $(1-\alpha)$ the following holds:

$$\mathbb{P}[s^-(t') \le \mathrm{RUL}(t') \le s^+(t')] = 1 - \alpha \tag{22}$$

where $\mathrm{RUL}(t') = T' - t'$ is the RUL in the transformed time. Therefore, one can write the left-hand side as $\mathbb{P}[t' + s^-(t') \le T' \le t' + s^+(t')]$. Using the transformation function g, which maps the original time scale to the transformed time scale, i.e., $t' = g(t)$ and $T' = g(T)$, and then substituting these into the probability expression and inverting, we obtain:

$$\mathbb{P}[g(t) + s^-(t') \le g(T) \le g(t) + s^+(t')] = \\ \mathbb{P}[g^{-1}(g(t) + s^-(t')) \le T \le g^{-1}(g(t) + s^+(t'))] \tag{23}$$

where the failure time in the original time is $T = g^{-1}(T')$ by definition. This provides a confidence interval for the end-of-life T, from which the following confidence interval for the RUL is derived:

$$\mathrm{RUL}(t) + t \in [g^{-1}(l), g^{-1}(u)] \tag{24}$$

where $l = g(t) + s^-(g(t))$ and $u = g(t) + s^+(g(t))$, with probability $(1-\alpha)$. A few simple algebraic manipulations of l and u result in the arguments of the inverse transformation g^{-1} defining both $L_\alpha(t)$ and $U_\alpha(t)$ in Theorem 1. Note that this requires the parameters μ and k to be known, or estimated accurately from data. Hence, these are usually affected by epistemic uncertainty, as mentioned in Section 4.1.

4.3.1. Added value of time transformation

One way of identifying the time transformation g consists of first fitting a parametric model for the reliability function $R(t)$. Alternatively, $g(t)$ can be obtained non-parametrically by applying Eq. (14) with cvn

estimated from the sample mean and the sample standard deviation of the time to failure. The parametric estimations are used in all case studies (Section 5), while in case study I the non-parametric method is illustrated as well, in Section 5.3. As compared to methods that rely on the reliability function, the proposed method explicitly evidences the factor k, which, in addition to its intuitive interest, often enables the derivation of an upper bound for the average RUL loss rate. From that bound, a lower bound on $MRL(t)$ can be derived.

4.4. Upper bound on average RUL loss rate

As already pointed out, Eq. (14) shows that the smaller the coefficient of variation $\frac{\sigma}{\mu}$, the steeper the slope k. In other words, a faster degradation corresponds to less uncertainty. Also, at the limit $t \to \infty$, the transformed time $t' \to \frac{\mu}{k}$. In many simple cases, such as when using parametric univariate distributions like the Weibull or Gamma, the $g(t)$ function is S-shaped and has an inflection point $t^\star$ where $\frac{\partial^2 g}{\partial t^2}$ vanishes. The time derivative can be seen as a metric for the speed of aging, and $t^\star$ marks the pivot from faster to slower aging. Before the inflection point, $g(t)$ is convex (faster aging), whilst after the inflection point it is concave (slower aging). The parameter k turns out to be an upper bound on the absolute value of the time derivative of the MRL, i.e., of the average RUL loss rate, after the inflection point:

$$\left|\frac{\partial v}{\partial t}\right| \leq k \quad \text{for} \quad t > t^\star \tag{25}$$

From Eq. (25) for $t^0 > t^\star$, there follows that, for $t > t^0 > t^\star$,

$$v(t) \geq v(t^0) - k(t - t^0) \tag{26}$$

assuming that $v(t)$ is convex (which is often true in practice and is guaranteed as long as $1/\lambda(t)$ is strictly convex [14]). When operational conditions change with time, even abruptly, this has an impact on the coefficient of variation and therefore on k and the transformation g. RUL estimations, along with the corresponding confidence interval, can be updated accordingly. For instance, for 2-parameter Weibull lifetimes, the value for k can be explicitly derived as,

$$k = \frac{2\Gamma^2(1+\beta^{-1})}{\Gamma(1+2\beta^{-1})} - 1 \tag{27}$$

where k is uniquely defined by the shape parameter β of the Weibull and Γ is Euler's Gamma function. Analogously, the parameter k for Gamma distributed lifetime is given by,

$$k = \frac{\beta - 1}{\beta + 1} \tag{28}$$

where β is the shape parameter of the Gamma distribution. In both cases, it is verified that, for a shape factor equal to 1, which corresponds to the exponential distribution, k is equal to 0; and, when $\beta \to \infty$, k converges to 1, corresponding to a deterministic (Dirac) distribution. Also note that, for Weibull distributed lifetimes, the inflection point t can be formally derived as follows:

$$t^\star = \eta \left(\frac{(\beta-1)}{\beta}\frac{(1-k)}{k}\right)^{\frac{1}{\beta}} \tag{29}$$

where η is the scale parameter. The proof is sketched in Appendix A. Fig. 3 illustrates $t^\star$, black dashed line, and the slope parameter k, blue solid line, as functions of the shape parameter β (x-axis). Note that both k and $t^\star$ are plotted on the y-axis and are calculated using Eqs. (29) and (27), respectively. Since the scale parameter η affects only the magnitude of $t^\star$, $\eta = 1$ is chosen to optimize the graphical output, i.e., by re-scaling $t^\star$ to a size comparable to $k \in [0, 1]$. The vertical lines and round markers show values of β, and the corresponding k, for the exponential case and the uniform case (in transformed time).

Determining inflection points for complex or unknown lifetime distributions is, however, not a simple task. Eq. (39) of Appendix A is the algebraic equation of which the inflection point $t^\star$ is a solution. It shows that, if the failure rate is a decreasing function of time (as in the Pareto distribution), the equation has no solution since the time derivative of lambda is then negative. Indeed, the $g(t)$ function has no inflection point in the case of the Pareto distribution. For complex distributions, multiple inflection points may be expected, corresponding to specific stages in the life of a system where degenerative changes occur. An illustration of this is provided in Section 5.2. However, the proposed framework can still be applied to such cases using nonparametric estimations of the reliability function $R(t)$, a transformation $g(t)$, and then determining $t^\star$ points as the set of times for which the second derivative of $g(t)$ vanishes. Those inflection points can be obtained by solving Eq. (39) iteratively, for instance with the Newton–Raphson method. Ensuring the numerical stability of the second derivative may require some smoothing or regularization to obtain reliable estimates, particularly in data-driven non-parametric settings. For a quantification of the effect of epistemic uncertainty on the $t^\star$ estimation, the interested reader is referred to Section 5.1, Effect of data volume.

4.5. Time transformations for degradation processes

The proposed approach naturally extends to stochastic degradation processes where end-of-life points are determined by lifetime boundaries and degradation thresholds rather than physical end-of-life events. Examples include the Wiener process with drift and the Gamma process, see [14] for additional details and examples. It has been seen that, to a random time to failure t, there corresponds a *time warping*, $g(t)$, defined by Eq. (18). In general, let $\{X(t)\}_{t\in T}$ denote a random degradation process with the time index t, and T_p the time for a degradation to reach a threshold p. Hence, for a threshold p, a lifetime random variable T_p and corresponding survival function R_p can be defined, i.e., the complementary CDF of the time for a degradation to reach threshold p. A family of time warping functions $\{g_p\}_{p\in P}$ which map each T_p into a transformed lifetime random variable $T'_p = g_p(T_p)$ with a linear MRL, can be defined as follows:

$$g_p(t) = \frac{\mu_p}{k_p}\left(1 - R_p(t)^{\frac{k_p}{1-k_p}}\right). \tag{30}$$

Thus, there will be a time transformation, g_p, with corresponding parameters μ_p and k_p associated with each degradation level p. The parameter μ_p is the average time to reach the degradation threshold p, and the parameter k_p is related to the coefficient of variation of that time.

As an illustration, consider the Wiener process with drift, characterized by the two parameters ν and σ, where ν is the average drift per unit of time (measured in units of degradation per unit of time) and σ^2 is the variance per unit of time, i.e., the variance of $X(t)$ is equal to $\sigma^2 t$. For instance, if the degradation were measured by the size of a crack, in meters, then ν would be measured in meters per hour (m/h), and σ^2 in square meters per hour (m^2/h). Then the first hitting time to degradation level p, T_p, has an inverse Gaussian distribution [57]. The expectation and variance of T_p are obtained, respectively, as $\mathbb{E}(T_p) = \frac{p}{\nu}$ and $\mathrm{Var}(T_p) = \frac{p\sigma^2}{\nu^3}$. These lead to an expression for k_p:

$$k_p = \frac{1 - \frac{\sigma^2}{\nu p}}{1 + \frac{\sigma^2}{\nu p}}. \tag{31}$$

Note that k_p must be non-negative, which, from (31), means that the inequality $\frac{\sigma^2}{\nu} \leq p$ must hold. Thus an appropriate time transformation g_p will exist for high enough degradation levels, and the constraint $\frac{\sigma^2}{\nu} \leq p$ amounts to imposing that, at any time t, the standard deviation of the degradation $X(t)$ does not exceed the average degradation (fluctuations are not too large). The constraint will be met for degradation levels p that are "not too small" and, indeed, the time to reach level p has a higher coefficient of variation for smaller p, since $cv(p) = \frac{\sigma}{(\nu p)^{0.5}}$. Nonetheless, as long as the condition $\frac{\sigma^2}{\nu} \leq p$ is met, the time transformation can be obtained from the reliability function of the inverse

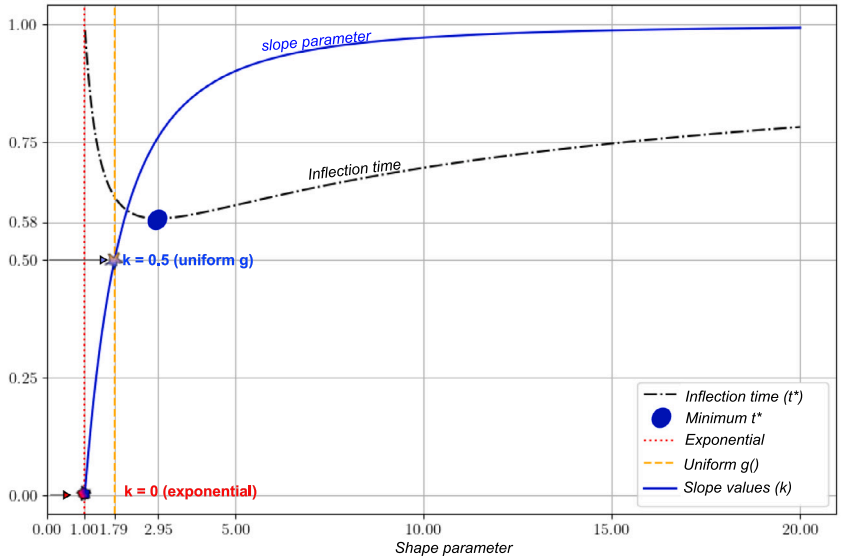


Fig. 3. Relationship between inflection point $t^\star$ and values of the shape parameter β for Weibull distributed lifetimes as per Eq. (29).

Gaussian variable. A closed-form expression for that reliability function can be found in [57]. From (31), it can be seen that k_p converges to 1 when either p goes to infinity (time to reach a very high degradation level), or ν goes to infinity (fast degradation process), or σ goes to zero (no fluctuations).

5. Case studies and numerical testing

First, we demonstrate the stability and robustness of the proposed procedure under increasing data volumes and across different parametric distribution families. We then illustrate its applicability to non-parametric mixture reliability models, exemplifying systems with heterogeneous populations. Next, to assess the practical effectiveness of the approach, we test and validate its efficacy in three realistic case studies. The goal is to predict the RUL of different components based on health and degradation indicators and quantify the uncertainty in the RUL predictions. The proposed methods are tested on the following real-world use cases,

(I) **LED-based lighting systems**: An assessment of the reliability of light-emitting diodes subject to accelerated degradation, see problem description and data in [30,58].
(II) **Sensor-equipped multi-component systems**: A reliability analysis of a fleet of four-component parallel systems equipped with sensors and operated under changing environments, as described in [7,37].
(III) **Aerospace propulsion systems**: RUL estimation and analysis of a fleet of commercial aircraft turbofans (N-CMAPPS data), as described in [38,59,60].

Note that all the use cases considered in this work are non-linear as they involve non-linear degradation processes. Hence, the MRL can be non-linear in the physical time (real time), and the property of linearity applies only to the transformed time $t' = g(t)$. This linearity is imposed by construction and represents a mathematical feature of the proposed approach. Therefore, it should not be viewed as a limitation of the proposed approach to real-world cases, which are typically non-linear and multi-modal.

5.1. Effect of data volume

Before discussing the problem setups and corresponding numerical outcomes, we first assess the stability and robustness of the proposed procedure using synthetic failure data from known failure distributions from different families. In particular, we aim to quantify the impact of epistemic uncertainty, stemming from limited failure data, through a data volume analysis. We examine how increasing the sample size influences the estimation of the slope coefficient k, the associated RUL interval $[s^-, s^-]$ in Eqs. (15)–(16), the transformation function $g(t)$, and the inflection point $t^\star$.

A non-parametric bootstrapping procedure is proposed as follows: For each sample size $n \in \{50, 100, \ldots, 1500\}$ (data volume), we use 500 bootstrap resamples of n time-to-failure data (Weibull- and Gamma-distributed). From each resample, a sample mean μ, coefficient of variation cv, corresponding k, see Eq. (14), and RUL bounds in the transformed time at a given α level are computed. Fig. 4 illustrates the results of this analysis for a Weibull case, where the increasing volume n is displayed on the x-axis. The 0.9 bootstrapped confidence intervals (CI) are presented in the 3 top panels for k, top left, s^+ in the center panel, and s^- on the right. A relative reduction in uncertainty, i.e., dividing the bootstrapped bound width by the largest bound $CI(n)/CI(50)$, is displayed in the bottom panel. The confidence intervals narrow as data volume increases, which reflects a reduction in epistemic uncertainty.

To better understand the impact of sample size on the estimation of the inflection point $t^\star$ we analyze the epistemic uncertainty associated with its estimation from time-to-failure data with varying volumes. This study quantifies how data volume influences the accuracy and confidence in the estimated $t^\star$ and $g(t)$. For this, randomized Gamma-distributed time-to-failure datasets were generated with sample sizes $n \in \{10, 50\}$, and scale and shape parameters of 5 and 20.9, respectively. Maximum likelihood estimation for the parameters was performed for all datasets, and $g(t)$ was computed, along with the corresponding $t^\star$. Fig. 5 presents the results of this analysis, with $n = 10$ in red and $n = 50$ in blue. The left panel shows the variability in the shape of $g(t)$ and the computed $(t^\star, g(t^\star))$ (displayed as markers enclosed within a convex hull). The right plot displays the distribution of $t^\star$ and the 99% confidence interval. A reduction in epistemic uncertainty is observed when more data is available, which is due to our ability to more accurately characterize and model $R(t)$ and $g(t)$. In this last example, the width of the 99% bootstrapped confidence interval on $t^\star$ decreases from between 40–71 h to a lower interval 48–63 h when increasing the data volume from 10 samples to 50 samples. The results highlight that larger sample sizes reduce uncertainty and improve the reliability of the proposed inflection point estimation, while smaller datasets introduce significant variability in the result.

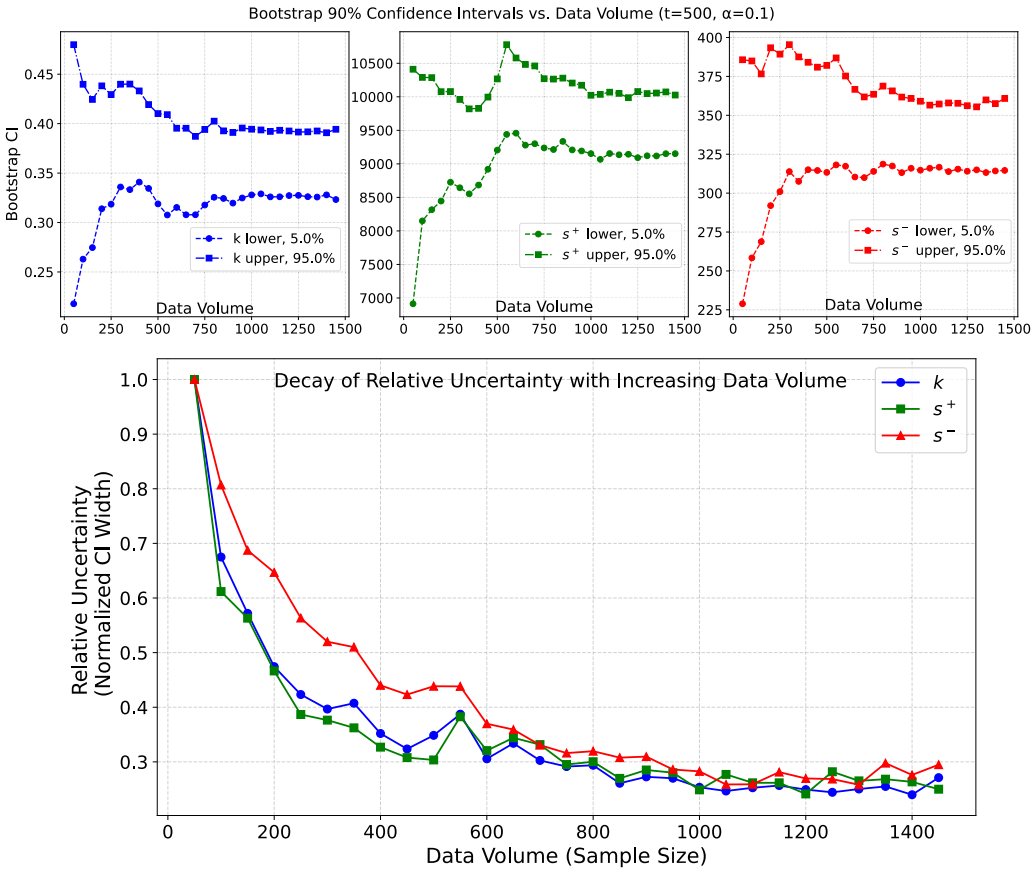


Fig. 4. Effect of data volume on the slope parameter k (top left), RUL bounds s^+ and s^- (top center and right), and relative reduction in the uncertainty (bottom panel).

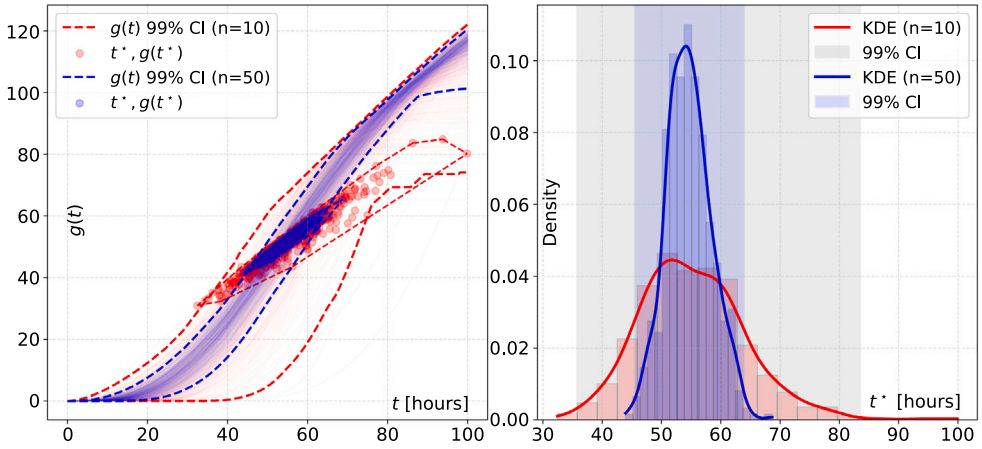


Fig. 5. Epistemic uncertainty associated with inflection point for Gamma-distributed lifetime data. On the left: the function $g(t)$ and inflection point $t^\star$ for $n = 10$ (red) and $n = 50$ (blue). On the right: the distribution of $t^\star$.

It is important to note that distributional assumptions are used solely for generating TTF samples, not for deriving the RUL bounds as outlined in the proposed method. This further highlights the generality of this new approach and its applicability independently of the distribution family $R(t)$, i.e., distribution-free.

5.2. Application to a non-parametric mixture problem

In real-world PHM applications, degradation behavior often varies across sub-populations, resulting in multi-modal, discontinuous, and non-parametric failure-time distributions. To evaluate the proposed method under such conditions, we simulate a heterogeneous population lifetime by using a mixture of three unknown distributions (Weibull, Beta, and Normal), each representing a distinct failure mode. A kernel density estimate is used to approximate the probability density function, with bandwidth selected via Silverman's rule. The reliability function $R(t)$ is derived from the KDE, and the time transformation $g(t)$ is computed as in Eq. (18), using the estimated slope coefficient k from the sample coefficient of variation cv. Fig. 6 illustrates how the transformation maps the complex MRL (non-monotonic in this example) in physical time into a linear trend in transformed time. Inflection points in $g(t)$ indicate shifts in degradation dynamics, adding interpretability

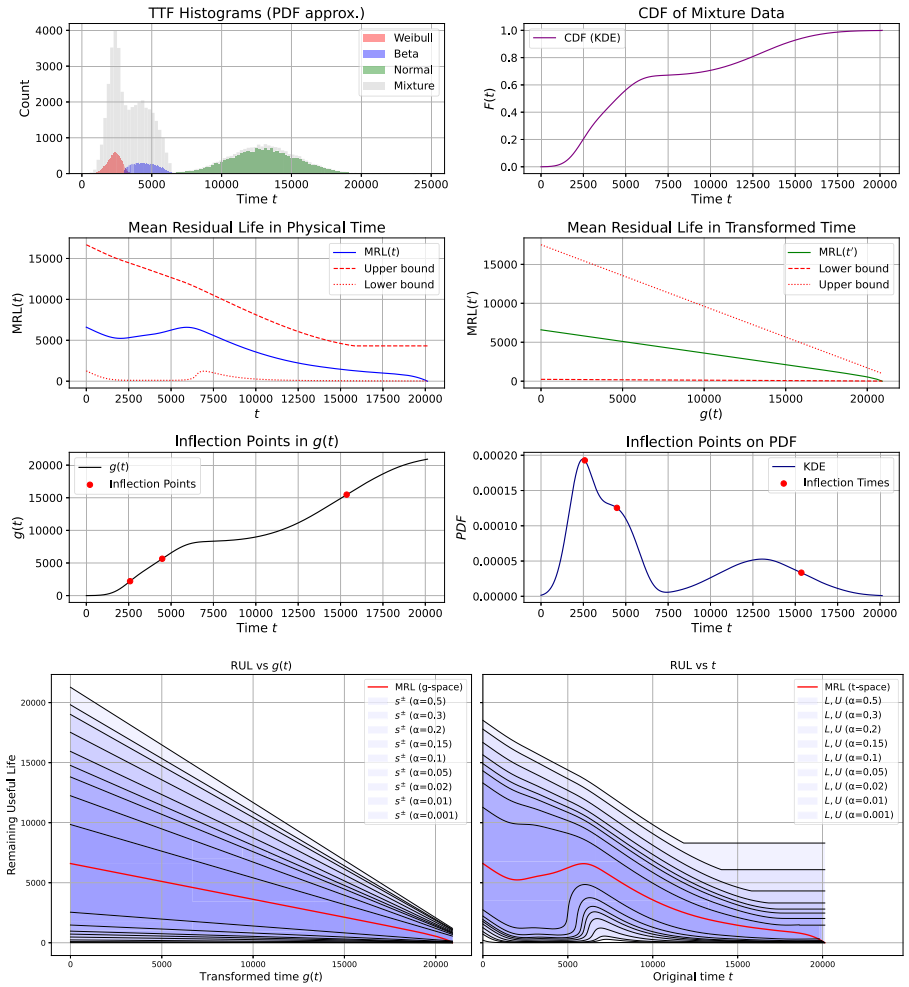


Fig. 6. Visualization of a nonparametric mixture model. From top to bottom panels: input distributions (top left), KDE-based cumulative distribution function (top right), MRL in physical and transformed time, transformation $g(t)$ with three inflection points (red markers) mapped to the estimated lifetime KDE density (right), MRL in the transformed time $g(t)$, and RUL confidence bounds for different α levels (bottom left), and MRL(t).

to otherwise opaque wear-out behavior. This analysis demonstrates the method's robustness in addressing non-parametric and complex distributions, and multi-modal degradation without assuming known component-level models, making it applicable for data-driven PHM of complex systems.

5.3. Case study I: LED reliability

The first use case evaluates LED package reliability by measuring luminous flux loss, which reflects lumen depreciation. Data was gathered under accelerated stress conditions $(\tau, I)_s$, with high temperature and current uniformly applied to batches of N components, refer to [30,58] for more details. Degradation-induced failures are identified when the normalized flux $\frac{X(t)}{X(0)} \leq p$, where p is an unacceptable depreciation level, typically 10 to 30%. Flux measurements are normalized at time zero, and the degradation trajectory is represented as $\mathbf{X} = \{X_t\}_{t=1}^{T}$, with $X_0 = 1$. The data for this case study is given by:

$$\mathcal{D}_1 = \left\{ \{\mathbf{X}_{j,s}\}_{j=1}^{25}; \tau_s, I_s \right\}_{s=1}^{4}, \tag{32}$$

where $\mathbf{X}_{j,s}$ denotes flux degradation trajectories for $j = 1, \ldots, 25$ LEDs under stress condition s. This dataset includes degradation measurements sampled monthly over 9072 h, testing 100 LEDs, 25 per stress condition, across 4 combinations of accelerated current and temperature.

5.3.1. The TM-21 baseline flux depreciation model

An Arrhenius inverse power law model is selected in this work to characterize thermoelectric aging effects on lumen maintenance due to its wide adoption in the research community, see e.g., [30,61,62]. The exponential flux depreciation model is defined by industrial standards as follows [62]:

$$X(t) = X(0)e^{-\lambda t} \tag{33}$$

where λ is the decay rate and $X(0)$ is the nominal flux at time zero. The Black model combines the effect of temperature and current on the rate λ and is defined as follows [63,64]:

$$\lambda(\tau, I) = C I^a e^{-E_a/(K_b \tau)}, \tag{34}$$

where τ is the temperature in Kelvin, $K_b = 8.617 \times 10^{-5}$ is the Boltzmann constant expressed in eV/K, E_a is the activation energy in eV, and C is a constant fitting parameter; a is a power coefficient to be estimated. Note that the effect of high forward currents I on the flux degradation is characterized by a power-law model whilst the effect of high temperature is quantified by the classical Arrhenius model. By combining (34) and (33), the following physics-based model for the first passage time (lifetime) can be derived as follows [65]:

$$T_p(\tau, I) = \frac{\log(1/p)}{C I^a e^{-E_a/(K_b \tau)}} \tag{35}$$

where T_p is the lifetime for a flux threshold p. Finally, by taking the logarithm of (35) and applying Eq. (34), a linearized inverse power

Table 1
Result of the lifetime analysis and best-fitting distributions according to the Akaike Information Criterion. The W stands for Weibull, and G for Gamma. Non-parametric estimation of k from sample mean and variance (cv) are also presented.

τ [°C]	85		105	85	105
I [A]	0.35		0.35	0.7	0.7
Best-fit	G	W	G	W	W
η [h]	–	7581	–	4934	3347
λ [h^{-1}] $\times 10^{-3}$	1.0	–	0.9	–	–
β	6.98	2.86	3.88	3.85	3.58
m [h] $\times 10^3$	6.82	6.75	4.45	4.46	3.01
$t^\star$ [h] $\times 10^3$	4.45		2.91	2.94	1.90
k (param)	0.75		0.59	0.84	0.82
k (non-par)	0.85		0.55	0.87	0.84

Table 2
RUL bounds in hours, for a confidence level $1-\alpha = 0.80$ and for the stress combination $I = 0.7$ [A] and $\tau = 85$ [°C].

t [h]	0	3000	4000	5000
$U_\alpha(t)$ [h]	6127	3227	2415	1757
$v(t)$ [h]	4463	1796	1232	841
$L_\alpha(t)$ [h]	2750	451	226	125

Table 3
Mean RUL, quantiles, and bounds on the expected RUL value, for 80% confidence level, predicted by the baseline model. Lifetime is defined at a degradation level $p = 0.98$. The results are for the stress condition $\tau = 85$ [°C] and $I = 0.7$ [A].

t [h]	0	2000	3000	4000	5000
$F^{-1}_{RUL}(0.9)$ [h]	9119	7119	6119	5118	4118
$v(t)$ [h]	4419	2419	1419	419	0
$F^{-1}_{RUL}(0.1)$ [h]	2099	99	0	0	0

law model can be obtained as follows [61]:

$$y = \theta \mathbf{z}^\intercal + \epsilon, \tag{36}$$

where $y = \log(\log(X(t)))$ is the iterated logarithm of the flux decay, $\theta = (\theta_0, \theta_1, \theta_2, \theta_3)$ are fitting parameters, and $\mathbf{z} = \left(1, \log(t), \frac{1}{\tau}, \log(I)\right)$ is a transformation of the explanatory variables (time, temperature and current). In this work, similarly to [30], the empirical distribution of the regression residuals F_ϵ is used to characterize "conventionally" the aleatoric uncertainty affecting the flux degradation trajectories and the extrapolated, T_p, and RUL.

5.3.2. Results and comparison

The method presented in Section 4 is applied to case study I. A high flux depreciation threshold $p = 0.98$ is assumed, implying an unacceptable performance when the LED's flux exceeds a 2% depreciation of the nominal value, i.e., when $X(t) < 0.98X(0)$. We compute lifetimes $T_{p=0.98}$ from 100 flux depreciation trajectories of identical LEDs, one for each device and stress condition. Note that the selected failure threshold is relatively harsh compared to the most common industry best practice of 50 to 90% and was chosen to reduce the right-censoring rate (due to highly durable LEDs). Table 1 shows the results of this analysis and the best-fitting distributions. An example of the time transformation $g(t)$ and $\frac{\partial g}{\partial t}$ are plotted in Fig. 7 for the stress level $I = 0.7$ [A] and $\tau = 85$ [°C]. Note that for the lower stress levels $I = 0.35$ [A], the inflection point corresponds to $t^\star = 4455$ [h], which indicates that $|\frac{\partial v}{\partial t}| \leq 0.75$ for $t > 4455$ [h]. On the other hand, for the same temperature but a higher stress current 0.7 [A], see Fig. 7, $k = 0.84$ and change from fast to slow aging occurs at $t^\star = 2940$ [h], which indicates the flux degradation stabilizes earlier: $|\frac{\partial v}{\partial t}| \leq 0.84$ for $t > 2940$ [h].

The method enables the derivation of confidence intervals for the RUL (see Table 2 in the Weibull case for a particular stress combination), which can support risk-based maintenance optimization. A Gamma model for the same value of k would lead to very close results, as the warping functions would be similar. Under continuous monitoring conditions, the k parameter could be updated with time, leading to narrower confidence intervals as increased degradation would result in higher values of k. The degradation, i.e., loss of LED luminous flux, could also be modeled by a Gamma or a Wiener process. For comparison, non-parametric estimates of k based on the sample mean and coefficient of variation (cv) are also reported in the last row of Table 1. The results of this estimation are comparable to the ones obtained using parametric models, except at the lowest stressor level (0.85 vs. 0.75 for non-parametric vs. parametric), due to the lower stress: more LED components passed the test without failing, and increased censoring. While parametric models account for censoring via maximum likelihood, the sample-based cv does not. This can be addressed by using non-parametric estimators that handle censoring, such as Kaplan–Meier, and deriving k from the resulting cv [66].

We compare the proposed method to the well-established flux degradation model described by the Illuminating Engineering Society of North America. Eq. (36) defines this traditional method. The mean RUL is extrapolated from the fitted model $X(t;\theta)$, and only one accelerated stress condition $\tau = 85$ [°C] and $I = 0.7$ [A] is considered to simplify the comparison. RUL prediction bounds are obtained similarly to [30]. Specifically, the 10th and 90th quantiles of the regression residual distribution, F_ϵ, establish an uncertainty band around the flux degradation trajectory as $[X(t;\theta)+F^{-1}_\epsilon(0.1), X(t;\theta)+F^{-1}_\epsilon(0.9)]$. The RUL intervals are then determined by intersecting the degradation band with the selected threshold $p = 0.98$. Table 3 shows the results of this analysis. Note that the prediction intervals from this approach are quite conservative, with lower bounds on the RUL quickly approaching zero for components tested beyond 2000 h under accelerated conditions. This issue was not observed with the proposed method. Additionally, a low degradation of the LEDs hinders the effectiveness of the regression method, leading to physically unrealistic estimations of model parameters θ, specifically, the activation energy E_a, which is directly related to the LEDs aging.

5.4. Case study II: Parallel systems

The second case study examines the reliability of a fleet of N parallel systems, each with four non-repairable components operating under diverse environmental conditions, from mild to harsh. For simplicity, sensor data are not considered here and the system's health is represented by a binary matrix $\mathbf{Y} = (\mathbf{y}_1, \ldots, \mathbf{y}_\mathcal{T})$, where each state vector $\mathbf{y}_t = (y_1, \ldots, y_4) \in \{0,1\}^4$ and $y_{i,t} = 0$ indicates a failure of component i at time t. For more details, refer to [37], and for insights on hybrid PHM solutions and data fusion, see [7,67]. The data for this case study is given by $D_2 = \{\mathbf{Y}_i\}_{i=1}^N$, where $\mathbf{Y}_i$ is the state matrix for the ith system. The lifetime L_i is determined as the earliest time when all components have failed, resulting in a dataset with N, partially right-censored lifetimes.

5.4.1. Results

The proposed approach is applied to use case II, and results are summarized in Fig. 8. The results for component one (the other components behave similarly) and for the composite system are displayed, respectively, on the left and right panels. The best fit for the component failure data is a 3-parameter Weibull distribution, while a gamma distribution better represents the reliability of the composite system. For the 3-parameter (shifted) Weibull distribution, by definition, no failure may occur before the shift parameter γ, which ranges from 777 [h] to 814 [h] for the four components. A key insight from our method is that the slope k is very close to 1, ranging from 0.967 to 0.99 for the various components, which suggests a quasi-deterministic failure process closely resembling a Dirac distribution. The quadruple redundancy

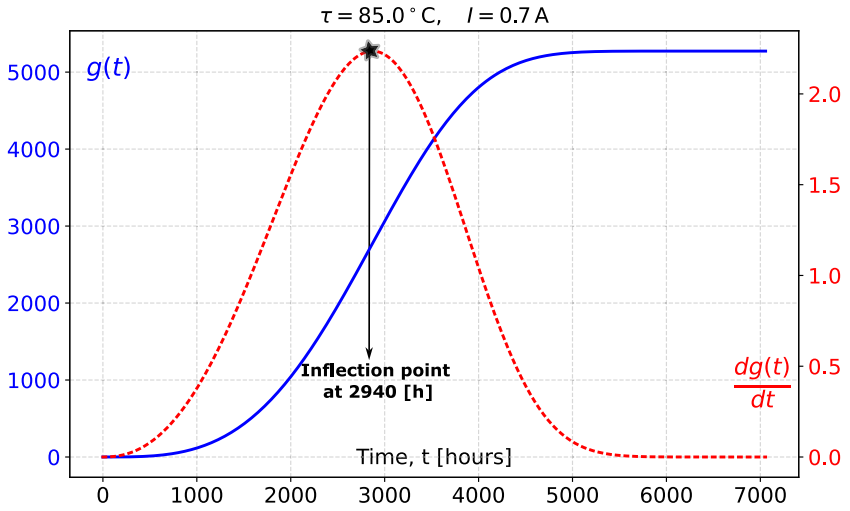


Fig. 7. The transformation function $g(t)$, dashed blue line, and its time derivative $\frac{\partial g}{\partial t}$, solid red line, for $I = 0.7$ [A] and $\tau = 85$ [°C].

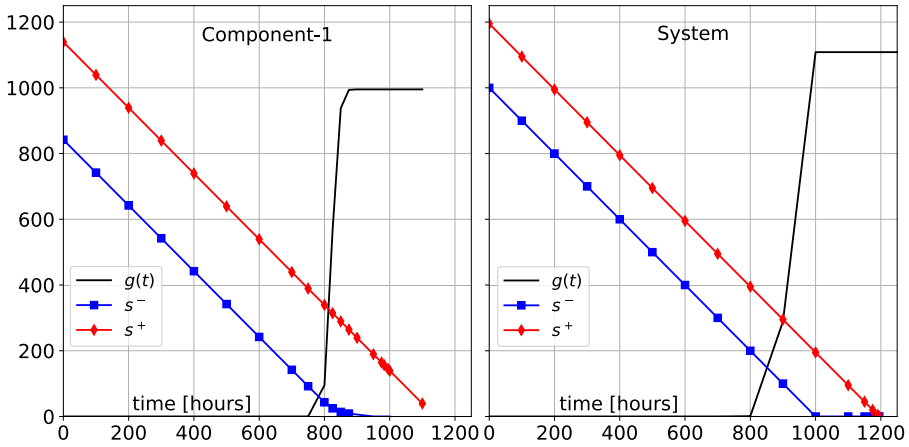


Fig. 8. The RUL confidence intervals and quasi step $g(t)$ for component 1 and the system.

achieves only a marginal increase in MTTF, that is, from 1003 [h] for the most reliable component to 1109 [h] for the whole system. This means that the four components are far from being independent and that common-cause failures/anomalies eliminate the beneficial effect of redundancy.

5.5. Case study III: Aircraft turbofan

The third case study examines a fleet of commercial aircraft turbofans, as described in [59,60]. The data is sourced from the N-CMAPPS dataset (DS003) [38], which includes complete degradation trajectories until failure for a dataset characterized by a failure mode impacting the efficiency and flows of both low-pressure and high-pressure turbines. A health index (HI) was calculated through a nonlinear mapping of operational margins under reference conditions [59]. Statistical analysis of the HI [68] demonstrated that the time to failure, i.e., the time needed for the HI to reach the value 0, is accurately modeled by a Weibull distribution with shape parameter $\beta = 7.32$ and scale $\eta = 77$ h. The HI could be approximated accurately by a power law [60], $\mathrm{HI}(t) = 1 - bt^c$, where the coefficient b is distributed as a Fréchet (inverse Weibull) random variable and the coefficient c was estimated by linear regression to be $c = 3.36$. Moreover, it was demonstrated [60] that the time T_p for the health index to reach an intermediate degradation level p is Weibull-distributed with the same shape parameter β as the TTF and a scale parameter η_p as a function of the degradation level, expressed as:

$$\eta_p = (1-p)^{1/c} \tag{37}$$

Based on these results, confidence intervals can now be derived, not only for the RUL, but also for the remaining time to reach a given degradation level. To this end, the time warping function is first determined from Eq. (30), taking Eq. (37) into account:

$$g_p(t) = \frac{\mu_p}{k}\left(1 - \exp\left(-\frac{k}{1-k}\left(\frac{t}{\eta_p}\right)^{\beta}\right)\right), \tag{38}$$

where $\mu_p = \eta_p \Gamma\left(1 + \frac{1}{\beta}\right)$, and k is a function of β only, given by Eq. (27). It is found that $k = 0.9493$ corresponds to a small coefficient of variation $CV = 0.16$. The confidence interval for the time needed for the HI to reach degradation level p from time t, i.e., for $(T_p - t)$, is obtained from Theorem 1. Since $(T_p - t)$ represents the RUL at time t for the failure defined by "hitting level p", the inverse function g_p^{-1}, necessary to calculate the confidence bounds, is obtained easily from Eq. (38).

5.5.1. Results

The application of the proposed method to the third use case has led to the results summarized in Table 4. Although the best estimate of the Weibull shape parameter is 7.32 (as discussed in Section 5.5), we have selected a value of $\beta = 5$, which still falls within the 95% confidence interval for the estimate of β. This choice allows for better

Table 4
Dynamic evolution of the bounds $U_\alpha(t)$ and $L_\alpha(t)$ at 80% confidence, use case III, and for three degradation levels $p \in \{0, 0.5, 0.8\}$, where $p = 0$ indicates a total loss in functionality.

t [h]	0	10	20	30	40	50	60	70	$t^\star$	Distance $\mu_{T_p} - t^\star$
Degradation level $p = 0$, $\mu_{T_p} = 70.69$ [h]										
$U_\alpha(t)$	90.98	80.98	70.99	61.05	51.27	41.87	33.14	25.43	47.42	23.28
$L_\alpha(t)$	49.09	39.10	29.20	19.90	12.20	6.92	3.87	2.23		
Degradation level $p = 0.5$, $\mu_{T_p} = 57.48$ [h]										
$U_\alpha(t)$	73.97	63.97	53.99	44.13	33.97	25.95	18.56	12.89	38.56	18.93
$L_\alpha(t)$	39.92	29.93	20.17	11.67	5.90	2.89	1.49	0.82		
Degradation level $p = 0.8$, $\mu_{T_p} = 43.72$ [h]										
$U_\alpha(t)$	56.27	46.27	36.33	26.75	18.18	11.46	–	–	29.33	14.40
$L_\alpha(t)$	30.37	20.39	11.08	4.67	1.84	0.80	–	–		

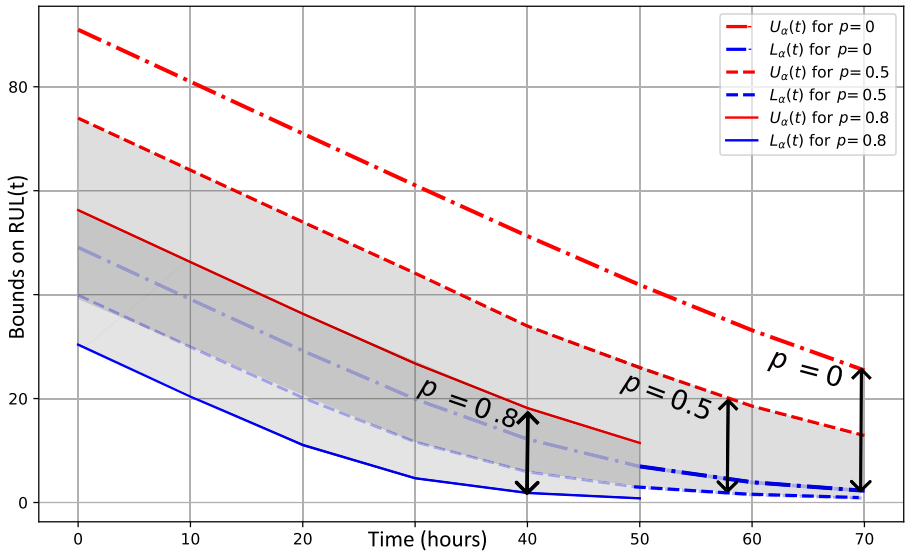


Fig. 9. Bounds $U_\alpha(t)$ and $L_\alpha(t)$ for three different degradation levels ($p = 0.8$, $p = 0.5$, and $p = 0$) with 80% confidence interval.

visualization of the results. The estimated value of k is 0.90 instead of 0.95. For three degradation levels $p \in \{0, 0.5, 0.8\}$, i.e., total failure, Table 4 provides the 80% confidence intervals for the time to reach the corresponding degradation level from any starting time between 0 and 70 h. For example, from time $t = 20$ h, the time to reach the degradation level $p = 0.8$ is between 11 and 36 h (with 80% probability), and the time to reach the degradation level $p = 0.5$ is between 21 and 54 h. Naturally, it takes more time to reach a higher degradation level (i.e., a lower value of p), so the bounds are decreasing functions of p. Additionally, for a given degradation level, the time required to reach it from a later starting point is shorter and less uncertain than from an earlier starting point. Thus, the bounds also decrease as functions of t, and the width of the confidence interval decreases with t. The MTTF, also denoted as $v(0)$, represents the average time to reach the selected degradation level starting from time 0. The confidence intervals are also illustrated in Fig. 9, where dash-dotted lines represent the confidence interval for $p = 0$, dashed lines for $p = 0.5$, and solid lines for $p = 0.8$.

5.5.2. Comparison with NN-based method

A comparison between the proposed method and the neural network methods referred to in [3,38,69] is presented next. The network is an asymmetric auto-encoder with the following characteristics: 1D-CNN layers. Hyperparameters: window size: 50, epochs: 20; batch size: 512, learning rate 10^{-4}; training protocol: supervised training; the network is trained to reconstruct sensor readings from, as inputs, sensor readings and operating conditions (see [3,38,69] for details). Table 5 shows the results of this comparison, where the average end of life T predicted by the neural network in [3] is compared against our method at different numbers of cycles (5, 15, 30, 45). The results are obtained by averaging over 6 different test samples. From this, the predicted MRL, $\hat{v}(t)$, is computed by subtracting the current number of cycles t from T. The absolute difference between that prediction and the ground truth is then calculated and displayed as the mean absolute error, denoted by Δ. The MRL predicted by our method shows superior accuracy, reducing the MAE sometimes by a significant margin, as shown in the last column, which reports the relative MAE variation ($rMAE$) in percentage. Unlike the NN method, our approach also provides a confidence interval, offering built-in UQ capabilities. Note that in [3], customized RUL predictions are generated for each sample; this is the added value of their method. In contrast, our method does not provide subject-specific predictions but offers the advantage of delivering accurate confidence intervals and quantifying uncertainty in the RUL distribution.

6. Discussion

The proposed method matches or exceeds the accuracy of current mainstream probabilistic approaches to RUL prediction, e.g., see [70–72], without requiring parametric assumptions. It supports general distributions via a non-parametric formulation (Section 5.2). Moreover, it makes the parameter k explicit, which allows derivation of an upper bound on the RUL loss rate and a lower bound on the mean residual life (Section 4.4). This enables dynamic updates of RUL estimates under changing operational conditions, as k and the warping transformation g adapt accordingly. The key novelty of this work lies in the analytical

Table 5
Comparison between NN in [3] and our method. Lifetime t expressed in number of cycles (ground truth MTTF, $\mu_T = 73$ cycles).

Ground truth		Approach in [3]		Proposed		$rMAE$ (%)
t	$\mathbb{E}[T]$ (MRL)	$\hat{v}(t)$	Δ (MAE)	$\hat{v}(t)$ (MRL)	Δ (MAE)	
5	68	70.8	2.8	65.5	2.5	−9.2
15	58	60.9	2.9	57.5	0.5	−83.0
30	43	47.1	4.1	40.5	2.5	−37.1
45	28	28.9	0.9	28.0	0.0	−100.0

approach proposed for obtaining confidence intervals of the estimated RUL and the derivation of inflection points separating faster and slower degradation periods. The availability of RUL estimates with associated confidence intervals and inflection points can be used to optimize maintenance schedules by balancing the costs of preventive inspections and potential costs due to equipment failures. Hence, this maintenance optimization conceptually entails imposing upper bounds on the probability that the RUL will be less than the time to the next inspection, thereby minimizing total expected costs (see [14] for details).

Our method also holds significance in accelerated life testing, aiding decision-making by deriving upper bounds on the average RUL loss rate and guiding optimal data collection strategies. Proactive maintenance strategies benefit from recognizing crucial junctures in the degradation process, when degradation shifts from fast to slow aging. Incorporating such insights could enhance the effectiveness of predictive maintenance. Future research could explore methods to anticipate and leverage precursor signals before inflection points, improving predictive maintenance's proactive nature. In our second case study, the inflection point occurs just before failure, indicating a sudden failure with little preceding insight. In case study 3, it is observed that the inflection point is quite distant from the MTTF and, as expected, even farther for higher degradation levels. Therefore, in this last example, it seems that a predictive maintenance strategy could be implemented and be beneficial. Thus, the relative location of the inflection point and MTTF or median RUL can be seen as an indicator of failure predictability, reflecting the presence of precursors.

7. Conclusion, limitations, and future directions

This paper introduced a novel dynamic method for the estimation of remaining useful life that explicitly quantifies aleatory uncertainty. This new method provides insights into how lifetime uncertainty evolves with aging dynamics, particularly through analytical characterization of the slope coefficient and inflection points in the transformed time domain. The applicability and efficacy of the method were demonstrated across several domains, including simple parametric problems with varying data volumes, an unknown non-parametric mixture reliability family, and three real-world engineering case studies. Hence, the method is broadly applicable to a wide range of domains, and the mathematical results shed new light on the dynamics of RUL, even for well-known lifetime distributions such as Weibull or Gamma. Thanks to the analytical computation of a slope coefficient and inflection points, new insights into how lifetime and RUL evolve dynamically are provided, and a better understanding of how aging speed affects lifetime uncertainty is obtained. The effects of epistemic uncertainty on the estimated parameters and the robustness of the proposed approach have been quantified numerically and discussed, with a focus on data volume and censoring. Although the current formulation focuses on univariate parametric time-to-failure distributions, it lays a solid foundation for future extensions. In particular, asset-specific RUL bounds influenced by varying environmental conditions, operational stressors, or mission profiles can be incorporated in future research.

To summarize, the current limitations and directions for future work include:

- **Dependence on failure data**: Estimating $R(t)$ requires sufficient coverage of failure-time distributions and a reliable mapping from degradation signals to time-to-failure labels. This can limit applicability during early deployment phases when failure data is scarce. Future work may explore models that learn directly from degradation signals, without requiring failure labels, and integrate adaptive or learned time-warping transformations into hybrid or deep learning frameworks for online inference. For instance, the use of recently suggested analytical health indices [60] can be contemplated.
- **Dynamic estimation of $g(t)$ and k**: The current method uses a static transformation. Future directions include dynamic estimation of the time-warping function and aging rate using advanced ML techniques, such as recurrent or physics-informed neural networks.
- **Concurrent degradation modes**: Many physical systems degrade through multiple, interacting mechanisms. Extending the framework to isolate and capture concurrent failure modes, each with distinct $g(t)$ and k, is essential for broader applicability.
- **Extension to multivariate cases and system-level and network PHM**: Extending the method to complex systems with dependencies or redundancies (e.g., networks or multi-component assets) is a promising direction. This could leverage system survival models and survival signatures [54,56] for multi-level reliability inference.
- **Modeling epistemic uncertainty**: While this work addresses aleatory uncertainty, epistemic uncertainty (e.g., due to limited data or model assumptions) is only quantified numerically via bootstrapping. Formal incorporation via generalized uncertainty theories or frameworks such as [55,73] could improve robustness. Also, real-world deployment must address incomplete and noisy data. Investigation of the robustness of the approach to various censoring (right, interval, or mixed), measurement errors, and other sources of epistemic uncertainty requires further work.
- **Covariates and non-stationary degradation**: The current model assumes survival function stationarity and does not include time-varying covariates influencing the lifetime distribution. Future extensions could account for external operational or environmental factors, and enable transformed piecewise-linear or regime-switching behaviors better capturing non-stationarity in $R(t)$ due to various wear dynamics.
- **Application to risk-based maintenance**: Integrating the proposed method into dynamic predictive maintenance and risk-based predictive maintenance frameworks, where failure risk is balanced against operational and maintenance costs, is a natural and impactful direction for future research.

Overall, this work establishes a formal and versatile framework for dynamic RUL estimation and uncertainty quantification, hence opening multiple avenues for future theoretical and applied research.

CRediT authorship contribution statement

Pierre Dersin: Writing – review & editing, Writing – original draft, Visualization, Resources, Project administration, Methodology, Investigation, Formal analysis, Conceptualization. **Roberto Rocchetta:** Writing – review & editing, Writing – original draft, Visualization, Project administration, Methodology, Investigation, Data curation, Conceptualization.

Software

To support reproducibility, an example implementation of the methods presented in this paper is publicly available at https://github.com/Roberock/TimeWarperRUL.git. The repository contains prototype code for the time warping algorithms, RUL bounds computation, and auxiliary utilities.

Declaration of competing interest

The authors declare that they have no known competing financial interests or personal relationships that could have appeared to influence the work reported in this paper.

Acknowledgments

The authors remember with profound emotion the intense and fruitful discussions on this topic with the late Prof. Dr. Alessandro Di Bucchianico in the spring of 2022. Also, thanks go to Dr. Manuel Arias-Chao and his team for feedback on some of the aspects of this research and for providing the material for case study III.

Appendix A. $t^\star$ for Weibull and Gamma distributions

The time transformation $g(t)$ is most often an S-shaped increasing function with one inflection point (see [14], chapter 6). In this appendix, a proof for $t^\star$ in the Weibull and Gamma distribution cases is highlighted. As per Eq. (6.22) in [14], the inflection point $t^\star$ is the solution of:

$$\frac{d\lambda}{dt} - \frac{k}{1-k}\lambda(t)^2 = 0. \tag{39}$$

Upon dividing both sides by $\lambda(t)$, (39) can be equivalently written as:

$$\frac{d\log\lambda}{dt} - \frac{k}{1-k}\lambda(t) = 0. \tag{40}$$

Upon substituting the explicit expression of the failure rate for a particular distribution in (40), the equation can be solved for $t^\star$. This is how the expression reported above, see Eq. (29), was derived in the Weibull distribution case [14]. For the Gamma case (see Eq. (5.47) of [14]), the slope of the linearized MRL is obtained from the parameter β as $k = \frac{\beta-1}{\beta+1}$. Therefore, $\frac{k}{1-k} = \frac{\beta-1}{2}$ and (40) can be written as:

$$\frac{d\log\lambda}{dt} - \frac{\beta-1}{2}\lambda(t) = 0. \tag{41}$$

In general, $\lambda(t) = -\frac{dR/dt}{R(t)} = \frac{f(t)}{R(t)}$, and, for a Gamma density $f(t)$,

$$\lambda(t) = \frac{1}{R(t)}\frac{\lambda}{\Gamma(\beta)}(\lambda t)^{\beta-1}e^{-\lambda t} \tag{42}$$

Therefore, the logarithm of the failure rate for a Gamma density is given by:

$$\log\lambda(t) = \log\lambda + (\beta-1)\log(\lambda t) - \lambda t - \log\Gamma(\beta) - \log R(t). \tag{43}$$

Hence, the first derivative of $\log\lambda(t)$ can be reduced to,

$$\frac{d\log\lambda(t)}{dt} = \frac{\beta-1}{t} - \lambda - \frac{dR/dt}{R(t)} = \tag{44}$$

$$= \frac{\beta-1}{t} - \lambda + \lambda(t). \tag{45}$$

Applying (45) to (41), $t^\star$ can be obtained as the solution of the following equation:

$$\frac{\beta-1}{t} - \lambda + \lambda(t) = \frac{\beta-1}{2}\lambda(t), \tag{46}$$

which can be further simplified as:

$$\beta - 1 - \lambda t = \frac{\beta-3}{2}\lambda(t)t. \tag{47}$$

Thus, $t^\star$ can be computed by solving Eq. (47), with $\lambda(t)$ given by Eq. (42). Note that for the exponential case, $\beta = 1$, and Eq. (47) is an identity. Similarly, for $\beta = 3$, the slope is given by $k = 1/2$, which corresponds to the uniform distribution. It follows from Eq. (47) that $t^\star = \frac{2}{\lambda}$, as the right-hand side vanishes. This result can also be obtained directly from $g(t)$ [14]. The corresponding time transformation function is plotted in Fig. 10 for $\lambda = 0.04781$/h, and for different shape parameters; it is verified for instance that, for $\beta = 3$, $t^\star = \frac{2}{\lambda} = 41.8$ h.

Appendix B. Derivation of moments

The definition of $g(t)$ implies that the reliability function is $R(t) = \left[1 - k\frac{g(t)}{\mu}\right]^{\frac{1-k}{k}}$, $0 \le t < \infty$. Given previous definitions, one can therefore write:

$$R'(t') = \left(1 - k\frac{t'}{\mu}\right)^{\frac{1-k}{k}}, \quad 0 \le t' < \frac{\mu}{k}, \tag{48}$$

which shows that the probability distribution of the random variable T', where

$$T' = g(T) \tag{49}$$

is that of a lifetime with an MRL linear in time t', with slope parameter k:

$$\nu'(t') = \mu - kt' \tag{50}$$

This formulation allows us to derive key statistical properties of the transformed lifetime T'. In particular, we show that $\mathbb{E}(T') = \mu$, and k is given in terms of the mean and variance of T, the time to failure in the initial referential. More generally, we derive expressions for the raw moments of $T' = g(T)$. Let α'_n denote the nth order raw moment of T', with distribution given by Eq. (48), and denoting the density by $f'(t) = -\frac{dR'}{dt}$ as usual:

$$\alpha'_n = \mathbb{E}[(T')^n] = \int_0^{\frac{\mu}{k}} s^n f'(s)ds \tag{51}$$

$$= \int_0^\infty g(t)^n f'(g(t))\frac{dg}{dt}dt. \tag{52}$$

Integrating by parts, and imposing $R'(g(t)) = R'(t') = R(t)$, we obtain $\alpha'_n = n\int_0^\infty g(t)^{n-1}R(t)\frac{dg}{dt}dt$. From the definition of $g(t)$, we differentiate to obtain:

$$\frac{dg}{dt} = \frac{\mu}{(1-k)}R(t)^{\frac{2k-1}{1-k}}f(t),$$

and therefore the nth order raw moment is given by:

$$\alpha'_n = n\frac{\mu}{(1-k)}\left(\frac{\mu}{k}\right)^{n-1}\int_0^\infty \left[1 - R(t)^{\frac{k}{1-k}}\right]^{n-1} R(t)^{\frac{k}{1-k}}f(t)dt.$$

Taking $x = R(t)$ as the integration variable,

$$\alpha'_n = \frac{n\mu^n}{k^{n-1}(1-k)}\int_0^1 \left[1 - x^{\frac{k}{1-k}}\right]^{n-1} x^{\frac{k}{1-k}}dx.$$

Using the change of variable $u = x^{\frac{k}{1-k}}$ (provided $0 < k < 1$), this reduces to

$$\alpha'_n = n\frac{\mu^n}{k^n}\int_0^1 u^{\frac{1}{k}-1}(1-u)^{n-1}du,$$

which can be expressed in terms of the Euler gamma function Γ as follows,

$$\alpha'_n = n\left(\frac{\mu^n}{k^n}\right)\frac{\Gamma(\frac{1}{k})\Gamma(n)}{\Gamma(\frac{1}{k}+n)}.$$

As n is an integer, $\Gamma(n) = (n-1)!$ and therefore, $\alpha'_n = n!\left(\frac{\mu}{k}\right)^n\frac{\Gamma(\frac{1}{k})}{\Gamma(\frac{1}{k}+n)}$. In particular, for $n = 1$, $\alpha'_1 = \mu$, that is, $E(T') = E(T)$. For $n = 2$, $\alpha'_2 = \frac{2\mu^2}{1+k}$, and therefore the variance of T' is equal to

$$Var(T') = \mathbb{E}(T'^2) - \mathbb{E}(T')^2 \tag{53}$$

$$= \frac{2\mu^2}{1+k} - \mu^2 = \frac{1-k}{1+k}\mu^2 = Var(T) \tag{54}$$

This confirms that the transformation $g(T)$ preserves the mean and variance of the original lifetime T.

Data availability

Data will be made available on request.

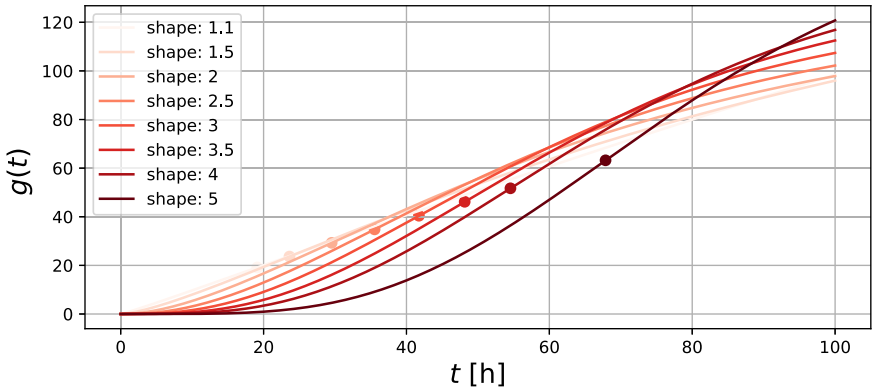


Fig. 10. Time transformation $g(t)$ for Gamma distribution with different shape parameters β and scale parameter $\lambda = 0.0478$ 1/h.

References

[1] Meeker W, Escobar L. Statistical methods for reliability data. New York: Wiley; 1998.

[2] Escobar LA, Meeker WQ. A review of accelerated test models. Statist Sci 2006;21(4):552–77. http://dx.doi.org/10.1214/088342306000000321.

[3] Arias Chao M, Kulkarni C, Goebel K, Fink O. Fusing physics-based and deep learning models for prognostics. Reliab Eng Syst Saf 2022;217:107961. http://dx.doi.org/10.1016/j.ress.2021.107961.

[4] Fan J, Yung KC, Pecht M. Physics-of-failure-based prognostics and health management for high-power white light-emitting diode lighting. IEEE Trans Device Mater Reliab 2011;11(3):407–16. http://dx.doi.org/10.1109/TDMR.2011.2157695.

[5] Rocchetta R, Broggi M, Huchet Q, Patelli E. On-line Bayesian model updating for structural health monitoring. Mech Syst Signal Process 2018;103:174–95. http://dx.doi.org/10.1016/j.ymssp.2017.10.015.

[6] Baraldi P, Cannarile F, Di Maio F, Zio E. Hierarchical k-nearest neighbours classification and binary differential evolution for fault diagnostics of automotive bearings operating under variable conditions. Eng Appl Artif Intell 2016;56:1–13. http://dx.doi.org/10.1016/j.engappai.2016.08.011.

[7] Rocchetta R, Gao Q, Mavroeidis D, Petkovic M. A robust model selection framework for fault detection and system health monitoring with limited failure examples: Heterogeneous data fusion and formal sensitivity bounds. Eng Appl Artif Intell 2022;114:105140. http://dx.doi.org/10.1016/j.engappai.2022.105140.

[8] Nejjar I, Geissmann F, Zhao M, Taal C, Fink O. Domain adaptation via alignment of operation profile for remaining useful lifetime prediction. 2023, arXiv preprint arXiv:2302.01704.

[9] Deng W, Nguyen T, Medjaher K, Gogu C, Morio J. Physics-informed machine learning in prognostics and health management: State of the art and challenges. Appl Math Model 2023. http://dx.doi.org/10.1016/j.apm.2023.07.011.

[10] Lei Y, Li N, Guo L, Li N, Yan T, Lin J. Machinery health prognostics: A systematic review from data acquisition to RUL prediction. Mech Syst Signal Process 2018;104:799–834. http://dx.doi.org/10.1016/j.ymssp.2017.11.016.

[11] Ferreira C, Gonçalves G. Remaining useful life prediction and challenges: A literature review on the use of machine learning methods. J Manuf Syst 2022;63:550–62.

[12] Fravolini ML, Costante G, Yucelen T, Napolitano MR. Interval prediction models for data-driven design of aerial vehicle's robust adaptive controllers. J Guid Control Dyn 2020;43(8):1512–28. http://dx.doi.org/10.2514/1.G004937.

[13] Sankararaman S, Daigle M, Saxena A, Goebel K. Analytical algorithms to quantify the uncertainty in remaining useful life prediction. In: 2013 IEEE aerospace conference. IEEE; 2013, p. 1–11.

[14] Dersin P. Modeling remaining useful life dynamics in reliability engineering. CRC press, Taylor & Francis; 2023.

[15] Mosallam A, Medjaher K, Zerhouni N. Data-driven prognostic method based on Bayesian approaches for direct remaining useful life prediction. J Intell Manuf 2016;27:1037–48.

[16] Kong D, Chen Y, Li N. Gaussian process regression for tool wear prediction. Mech Syst Signal Process 2018;104:556–74. http://dx.doi.org/10.1016/j.ymssp.2017.11.021.

[17] Wang S, Fan Y, Jin S, Takyi-Aninakwa P, Fernandez C. Improved anti-noise adaptive long short-term memory neural network modeling for the robust remaining useful life prediction of lithium-ion batteries. Reliab Eng Syst Saf 2023;230:108920.

[18] Tang T, Yuan H. A hybrid approach based on decomposition algorithm and neural network for remaining useful life prediction of lithium-ion battery. Reliab Eng Syst Saf 2022;217:108082.

[19] Nguyen KT, Medjaher K, Gogu C. Probabilistic deep learning methodology for uncertainty quantification of remaining useful lifetime of multi-component systems. Reliab Eng Syst Saf 2022;222:108383.

[20] Zio E, Di Maio F. A data-driven fuzzy approach for predicting the remaining useful life in dynamic failure scenarios of a nuclear system. Reliab Eng Syst Saf 2010;95(1):49–57. http://dx.doi.org/10.1016/j.ress.2009.08.001.

[21] Alamaniotis M, Grelle A, Tsoukalas LH. Regression to fuzziness method for estimation of remaining useful life in power plant components. Mech Syst Signal Process 2014;48(1):188–98. http://dx.doi.org/10.1016/j.ymssp.2014.02.014.

[22] Shaheen B, Kocsis Á, Németh I. Data-driven failure prediction and RUL estimation of mechanical components using accumulative artificial neural networks. Eng Appl Artif Intell 2023;119:105749.

[23] Ren L, Dong J, Wang X, Meng Z, Zhao L, Deen MJ. A data-driven auto-CNN-LSTM prediction model for lithium-ion battery remaining useful life. IEEE Trans Ind Inform 2020;17(5):3478–87.

[24] Anaby-Tavor A, Carmeli B, Goldbraich E, Kantor A, Kour G, Shlomov S, Tepper N, Zwerdling N. Do not have enough data? Deep learning to the rescue!. In: Proceedings of the AAAI conference on artificial intelligence. vol. 34, 2020, p. 7383–90.

[25] Al-Dahidi S, Di Maio F, Baraldi P, Zio E. Remaining useful life estimation in heterogeneous fleets working under variable operating conditions. Reliab Eng Syst Saf 2016;156:109–24.

[26] Rocchetta R, Broggi M, Patelli E. Do we have enough data? Robust reliability via uncertainty quantification. Appl Math Model 2018;54:710–21. http://dx.doi.org/10.1016/j.apm.2017.10.020.

[27] Fink O, Wang Q, Svensen M, Dersin P, Lee W-J, Ducoffe M. Potential, challenges and future directions for deep learning in prognostics and health management applications. Eng Appl Artif Intell 2020;92:103678. http://dx.doi.org/10.1016/j.engappai.2020.103678.

[28] Lathourakis C, Cicirello A. Physics enhanced sparse identification of dynamical systems with discontinuous nonlinearities. Nonlinear Dynam 2024;1–28.

[29] Cicirello A. Physics-enhanced machine learning: a position paper for dynamical systems investigations. 2024, arXiv preprint arXiv:2405.05987.

[30] Rocchetta R, Zhan Z, van Driel WD, Di Bucchianico A. Uncertainty analysis and interval prediction of LEDs lifetimes. Reliab Eng Syst Saf 2024;242:109715. http://dx.doi.org/10.1016/j.ress.2023.109715.

[31] Abdar M, Pourpanah F, Hussain S, Rezazadegan D, Liu L, Ghavamzadeh M, Fieguth P, Cao X, Khosravi A, Acharya UR, Others. A review of uncertainty quantification in deep learning: Techniques, applications and challenges. Inf Fusion 2021;76:243–97.

[32] Sankararaman S, Daigle MJ, Goebel K. Uncertainty quantification in remaining useful life prediction using first-order reliability methods. IEEE Trans Reliab 2014;63(2):603–19.

[33] Si X-S, Wang W, Hu C-H, Zhou D-H. Remaining useful life estimation–a review on the statistical data driven approaches. European J Oper Res 2011;213(1):1–14.

[34] Liu K, Shang Y, Ouyang Q, Widanage WD. A data-driven approach with uncertainty quantification for predicting future capacities and remaining useful life of lithium-ion battery. IEEE Trans Ind Electron 2020;68(4):3170–80.

[35] Hall W, Wellner JA. Estimation of mean residual life. Stat Model Biol Syst Mem Andrei Yakovlev 2020;169–89.

[36] Van Driel WD, Fan X. Solid state lighting reliability: components to systems, vol. 1, Springer Science & Business Media; 2012.

[37] Cannarile F, Compare M, Baraldi P, Yang Z, Zio E. The aramis challenge: prognostics and health management in evolving environments. 2020, Retrieved from ESREL2020-PSAM15: https://www.esrel2020-psam15.org/Aramis_Challenge.pdf.

[38] Arias Chao M, Kulkarni C, Goebel K, Fink O. Aircraft engine run-to-failure dataset under real flight conditions for prognostics and diagnostics. Data 2021;6(1):5.

[39] Chang M-H, Das D, Varde P, Pecht M. Light emitting diodes reliability review. Microelectron Reliab 2012;52(5):762–82. http://dx.doi.org/10.1016/j.microrel.2011.07.063.

[40] Barlow RE, Proschan F. Mathematical theory of reliability. SIAM; 1996.
[41] Nelson WB. Accelerated testing: statistical models, test plans, and data analysis. John Wiley & Sons; 2009.
[42] Zhang S, Yuan X, Wang H, Mérida W, Zhu H, Shen J, Wu S, Zhang J. A review of accelerated stress tests of MEA durability in PEM fuel cells. Int J Hydrog Energy 2009;34(1):388–404. http://dx.doi.org/10.1016/j.ijhydene.2008.10.012.
[43] Hao J, Li D, He C, Sun Q, Ke H. Step-down accelerated aging test for LED lamps based on Nelson models. Optik 2017;149:69–80. http://dx.doi.org/10.1016/j.ijleo.2017.09.018.
[44] Lall P, Wei J, Sakalaukus P. Bayesian probabilistic model for life prediction and fault mode classification of solid state luminaires. In: 2014 international conference on prognostics and health management. IEEE; 2014, p. 1–10.
[45] Nemani V, Biggio L, Huan X, Hu Z, Fink O, Tran A, Wang Y, Du X, Zhang X, Hu C. Uncertainty quantification in machine learning for engineering design and health prognostics: A tutorial. 2023, arXiv:2305.04933.
[46] Rocchetta R, Perrone E, Herzog A, Dersin P, Di Bucchianico A. A survey on LED prognostics and health management and uncertainty reduction. Microelectron Reliab 2024;157:115399. http://dx.doi.org/10.1016/j.microrel.2024.115399.
[47] Chen W-B, Li X-Y, Kang R. Integration for degradation analysis with multi-source ADT datasets considering dataset discrepancies and epistemic uncertainties. Reliab Eng Syst Saf 2022;222:108430. http://dx.doi.org/10.1016/j.ress.2022.108430.
[48] Xiahou T, Zeng Z, Liu Y. Remaining useful life prediction by fusing expert knowledge and condition monitoring information. IEEE Trans Ind Inform 2020;17(4):2653–63.
[49] Kobayashi K, Alam SB. Explainable, interpretable, and trustworthy AI for an intelligent digital twin: A case study on remaining useful life. Eng Appl Artif Intell 2024;129:107620. http://dx.doi.org/10.1016/j.engappai.2023.107620.
[50] Rigamonti M, Baraldi P, Zio E, Roychoudhury I, Goebel K, Poll S. Ensemble of optimized echo state networks for remaining useful life prediction. Neurocomputing 2018;281:121–38.
[51] Rocchetta R, Mey A, Oliehoek FA. A survey on scenario theory, complexity, and compression-based learning and generalization. IEEE Trans Neural Netw Learn Syst 2023;1–15. http://dx.doi.org/10.1109/TNNLS.2023.3308828.
[52] Campi MC, Garatti S. Compression, generalization and learning. J Mach Learn Res 2023;24(339):1–74.
[53] Hall W, Wellner JA. Estimation of mean residual life. Stat Relat Top 1981;169–83.
[54] Feng G, Patelli E, Beer M, Coolen FP. Imprecise system reliability and component importance based on survival signature. Reliab Eng Syst Saf 2016;150:116–25. http://dx.doi.org/10.1016/j.ress.2016.01.019.
[55] Beer M, Ferson S, Kreinovich V. Imprecise probabilities in engineering analyses. Mech Syst Signal Process 2013;37(1–2):4–29. http://dx.doi.org/10.1016/j.ymssp.2013.01.024.
[56] Shi Y, Behrensdorf J, Zhou J, Hu Y, Broggi M, Beer M. Network reliability analysis through survival signature and machine learning techniques. Reliab Eng Syst Saf 2024;242:109806. http://dx.doi.org/10.1016/j.ress.2023.109806.
[57] Chhikara RS, Folks JL. The inverse Gaussian distribution as a lifetime model. Technometrics 1977;19:461–8.
[58] Ibrahim MS, Fan J, Yung WKC, Prisacaru A, van Driel W, Fan X, Zhang G. Machine learning and digital twin driven diagnostics and prognostics of light-emitting diodes. Laser Photonics Rev 2020;14(12):2000254. http://dx.doi.org/10.1002/lpor.202000254.
[59] Bajarunas K, Baptista M, Goebel K, Chao MA. Unsupervised physics-informed health indicator estimation for complex systems. In: Annual conference of the PHM society. vol. 15, 2023, p. 1–12.
[60] Dersin P, Goglio D, Bajarunas K, Arias-Chao M. Analytical health indices: Towards reliability-informed deep learning for PHM. Int J Progn Health Manag 2025;16(2). http://dx.doi.org/10.36001/ijphm.2025.v16i2.4262.
[61] Dusmez S, Duran H, Akin B. Remaining useful lifetime estimation for thermally stressed power MOSFETs based on on-state resistance variation. IEEE Trans Ind Appl 2016;52(3):2554–63. http://dx.doi.org/10.1109/TIA.2016.2518127.
[62] Becky K, Andrew J, David N, Jianzhong o, Jiao and. ANSI/IES TM-35-19: Projecting long-term chromaticity coordinate shift of LED packages, arrays and modules. Tech. rep., Illuminating Engineering Society; 2019.
[63] Yang X, Sun B, Wang Z, Qian C, Ren Y, Yang D, Feng Q. An alternative lifetime model for white light emitting diodes under thermal–electrical stresses. Materials 2018;11.
[64] Tan K-Z, Lee S-K, Low H-C. LED lifetime prediction under thermal-electrical stress. IEEE Trans Device Mater Reliab 2021;21(3):310–9. http://dx.doi.org/10.1109/TDMR.2021.3085579.
[65] Fan J, Jing Z, Cao Y, Ibrahim MS, Li M, Fan X, Zhang G. Prognostics of radiation power degradation lifetime for ultraviolet light-emitting diodes using stochastic data-driven models. Energy AI 2021;4:100066. http://dx.doi.org/10.1016/j.egyai.2021.100066.
[66] Klein JP, Moeschberger ML. Survival analysis: techniques for censored and truncated data. Springer Science & Business Media; 2006.
[67] Zhao W, Yang L, Dang C, Rocchetta R, Valdebenito M, Moens D. Enriching stochastic model updating metrics: An efficient Bayesian approach using Bray-Curtis distance and an adaptive binning algorithm. Mech Syst Signal Process 2022;171:108889. http://dx.doi.org/10.1016/j.ymssp.2022.108889, URL https://www.sciencedirect.com/science/article/pii/S0888327022000796.
[68] Dersin P, Bajarunas K, Arias-Chao M. Analytical modeling of health indices for prognostics and health management. In: Annual conference of the PHM society. vol. 8, (1):2024, p. 176–85.
[69] Bajarunas K, Baptista ML, Goebel K, Chao MA. Health index estimation through integration of general knowledge with unsupervised learning. Reliab Eng Syst Saf 2024;251:110352. http://dx.doi.org/10.1016/j.ress.2024.110352.
[70] Jolfaei NG, Rameezdeen R, Gorjian N, Jin B, Chow CWK. Prognostic modelling for industrial asset health management. Saf Reliab 2022;41(1):45–97. http://dx.doi.org/10.1080/09617353.2022.2051140.
[71] Kahle W, Mercier S, Paroissin C. Degradation processes in reliability. John Wiley & Sons; 2016.
[72] Huynh KT, Grall A, Bérenguer C. Assessment of diagnostic and prognostic condition indices for efficient and robust maintenance decision-making of systems subject to stress corrosion cracking. Reliab Eng Syst Saf 2017;159:237–54.
[73] Shafer G. A mathematical theory of evidence turns 40. Internat J Approx Reason 2016;79:7–25. http://dx.doi.org/10.1016/j.ijar.2016.07.009.